Optical spectroscopy characterization of nano-scale photonic structures

A thesis submitted in fulfillment of the requirements for the degree of Master of Engineering

Hasan Qasim
B Tech

School of Electrical and Computer Engineering
RMIT University, Melbourne, Australia

March 2008

STATEMENT

The work presented within this thesis holds no material or information that has been accepted for the award in any university for any degree. To the best of my knowledge and belief, this thesis does not contain any material written by another person except for the places denoted by specific references. The content of this thesis is the product of research work carried out at RMIT University, since the starting of this research program.

Hasan Qasim

March 2008

ACKNOWLEDGEMENTS

The author would like to acknowledge important inputs given by the following persons or organizations during the entire course of research. I would like to:

- Extend my sincere thanks & gratitude to A/Professor Iouri Belski (my senior supervisor) & A/Professor Arnan Mitchell (my second supervisor), for their guidance, assistance and support through the entire research.
- Thank Sr. Lecturer Kourosh Kalantar-Zadeh, for his guidance through my research.
- Extend my warm thanks to research students who greatly helped me in my research especially Gorgi Kostovski, Rashidah Arsat, Abu Sadek to name a few.
- Thank RMIT (MMTC group's) technical staff for their help.
- Grateful to RMIT University Library, for providing me with ample amount of research related materials.
- Finally, I would like to thank my beloved family and friends for morally supporting me all the way through my research.

TABLE OF CONTENTS

LIST OF FIGURES

.

LIST OF TABLES

SUMMARY

Current micro-scale electronics technology has been approaching rapidly towards its technological limit. This has shifted the focus towards nano-scale technology in recent years. More and more researchers around the globe are working in pursuit of bringing nano-scale technology into mainstream.

The research carried out here is a small step towards a similar goal. The remarkable optical properties exhibited by certain nano-scale structures are in stark contrast to their bulk form and this provides the basis for this research.

Two kinds of nanostructures are developed and investigated for their optical properties. One of these is nanofibers processed from a polymer known as polyaniline (PANI). The focus of this study is to investigate its optical and conductive properties under different conditions of doping environments, temperature and polymerization conditions. Optical characterization technique such as UV-Visible spectroscopy is developed to carry out the investigation. The developed nanofibers have been demonstrated to possess optical and conductive properties to be dependent on doping variables. Study of these optical properties could prove very useful in the development of electrochromic devices and gas sensors. Later in the research, UV-Visible spectroscopy has been improved into a low cost Raman spectroscopy setup which is validated by experimentation carried out on some samples.

The second type of nano-structure developed and investigated, is an array of nanoparticles of noble metals such as gold and silver. Such an array is shown to exhibit a phenomenon called **plasmon resonance effect** when excited by light. UV-Visible spectroscopy technique is utilized to investigate this effect for metal nano-arrays. A biologically nano-structured surface (wing of an insect called cicada) is used as the substrate for the fabrication of metal array. A serious attempt has also been made to do '**Surface Enhanced Raman Spectroscopy (SERS)',** making use of the metal nano-array developed. This technique improves the raman lines intensities of certain less sensitive samples such as thiophenol, which are known to give weak raman lines. This is carried out by adsorbing the sample on the metal nano-array.

Chapter1 Introduction

1.1 Introduction

The research described in this thesis is a little step combining the worlds of photonics and nanotechnology. It revolves around two kinds of nanostructured materials, one of which obtained from nature is a wing of an insect called cicada and is being used to develop nanostructured metal arrays, while the other being developed and investigated by researchers are polymeric nanofibers. The concept behind these nanostructures is obtained from literature (Sengupta, 2006; Liu, 2003; Watson, 2002; Aliganga, 2006 and Daniel, 2004) and the work is extended and is novel in certain ways.

This research carries out an investigation of these nanostructures to establish certain remarkable optical properties of these nanostructures which differ significantly from the bulk properties of the materials being used to prepare nanostructures.

In this chapter, the motivation that paved way for this research is talked about followed by set objectives and approach undertaken for this research. Lastly, each chapter is summarised in a few sentences each.

1.2 Motivation

In anticipation of the pace of development of electronics, nano-scale electronics has become the focus of many researchers and engineers in academia and industry since early 1990s (Waser, 2005 and Frahner, 2004). Basic building blocks of modern integrated circuits have been diodes and transistors and there is constant vigil to decrease their sizes further.

A unique aspect of nanotechnology is the vastly increased ratio of surface area to volume present in many nano-scale materials. New generation of analytical tools such as the atomic force microscope (AFM), and the scanning tunneling microscope (STM), scanning electron microscope (SEM), combined with processes such as electron beam lithography and molecular beam epitaxy, allow deliberate manipulation of nanostructures, and leads to the observation of novel phenomena. A number of

physical phenomena for example the “quantum size effect” where the electronic properties of solids are altered with great reductions in particle size become noticeably pronounced. Additionally, a number of physical properties such as optical properties change when compared to macroscopic systems for example the behavior of such materials towards light (Goser, 2004).

An example for the change in optical property could be of nano-particles made of noble metal such as gold. The bulk form of gold is known to give a wavelength band in the UV range of electromagnetic radiation which imparts it a shiny appearance (Berciaud, 2005). But as the size is reduced and particles of gold are produced in the nano-scale range, the optical properties are found to change tremendously. A layer of gold nanoparticles begin to appear green in color when observed under a microscope.

The optical property of gold nanoparticles is just one example to state that materials reduced to the nano-scale can show very different properties compared to what they exhibit on a macro or micro-scale, enabling unique applications. As such nano-crystalline systems have attracted our interest for this research due to their novel optical properties.

Some of the contributing factors to these properties can include quantum confinement of energy carriers such as photons within nanoparticles as happens for ‘surface plasmon resonance’ effect discussed in chapter 5, efficient energy and charge transfer over nano-scale distances as for polyaniline nanofibers discussed in chapter 3. With the growing technology of these materials, it becomes increasingly necessary to understand the detailed basis for their nanophotonic properties. The linear and nonlinear optical properties of such materials can be finely tailored by controlling the crystal dimensions and orientations, chemistry of their surfaces, the fabrication technology and the environment conditions such as doping medium and temperature.

Thus, it gives enough motivation to investigate the processes leading to such remarkable photonic properties of nano-scale structures, through experimentation.

1.3 Objective and approach

The main objectives drafted for this research include:

1. Learn to prepare and develop certain nano-scale structures.
2. Develop certain optical spectroscopy techniques to investigate the optical properties of prepared nanosize structures.

The nano-scale structures that have been investigated in this research here include:

1. Nanometric fibers of a conductive polymer known as polyaniline.
2. Metallic nanoparticle arrays based on a biological substrate.

These two though being very different kinds of nanostructures, they have been studied together in this research and can be combined as surface or interface nano-structures for photonics applications. These nano-structures exhibit remarkable optical properties which are very different from their bulk properties. For this purpose, two optical spectroscopy instrumentation techniques have been developed as part of this research, namely UV-Visible and Raman.

The research first develops nanofibers of polyaniline and device a UV-Visible spectroscopy setup to investigate its optical property which are ultimately proven to be a function of its doping levels, temperature and electrolytic environment. Research then moves to develop an advanced type of spectroscopy instrumentation which is called Raman spectroscopy. This instrumentation is developed and validated by carrying out experimentation on samples of paracetamol and polystyrene. The obtained results are compared with those published in references.

Having established both UV-Visible and Raman spectroscopy, both the techniques are then utilized to investigate optical properties of yet another kind of nanostructures which is an array of metal nanostructures based on a biological substrate. The results are obtained for plasmon resonance effect dependency on size of nanoparticles. Results obtained for SERS are not very informative, thus could pave way for future research endeavors.

1.4 Summary of Chapters

To document the details of this research, this thesis has been organized in 6 chapters as:

Chapter 2 lays foundation of this research through a literature review which discusses some of the work done by authors and is similar to the work done by us in certain ways. Essential conceptual understanding of aspects around which the thesis revolves, is developed through the literature review. Literature review is divided into three major areas of study.

Chapter 3 begins describing the research. To start with, UV-Visible spectroscopy technique is developed and validated by obtaining a reflection spectrum for a sample of a 'thin film' device. The chapter then deals with formulation of polymer fibers which are shown to be of nanometer scale in diameters. Polyaniline in nanofibric form is shown to possess remarkable optical properties; more specifically it shows inter-conversion of color with the doping and dedoping process. This property is being exploited in development of electrochromic windows and devices. UV-Visible spectroscopic measurements are done to investigate this property as a function of doping and dedoping. The results obtained give conclusive evidence to this property. Also, electrical conductivity is shown to be influenced by doping process.

Chapter 4 connects to previous chapter in the sense that it takes optical spectroscopy one step further from UV-Visible and describes a more renowned and advanced form known as Raman spectroscopy. Raman spectroscopy is known to provide a vast amount of information regarding molecular properties such as the presence of various functional groups in a molecule, the bond lengths etc. The understanding developed in literature review is made use in developing a custom made system which is though not among the superior systems as far as sensitivity and optical resolution goes but definitely among more cost-effective ones. Various parts and components of the system are also described explicitly. It is validated by examples of an as-obtained tablet of paracetamol which is chemically a para-substituted

benzene molecule. Another sample investigated is of polystyrene which is commonly used plastic product. Lastly, the chapter also discusses a major drawback when doing raman spectroscopy called fluorescence and possible ways of its eradication.

Chapter 5 moves towards discussing another kind of nano-scale structure that has become the talking point of many researchers lately due to its amazing optical properties. It investigates the surface plasmon resonance as obtained from an array of metallic nanoparticles such as gold and silver. As said before, such an array shows optical properties different from the bulk particles. The understanding from literature review is useful in explaining the mechanism and results obtained. Again, UV-Visible spectroscopy is used to obtain plasmon frequency bands as a function of size of these nanoparticles. The chapter then investigates another remarkable property that can be obtained from such an array. This property known as surface enhanced raman, is utilized to obtain raman spectrum of substance which gives weak Raman signal is adsorbed on the surface of the metal array. The Raman spectroscopy is done and the signal is as the name indicates is vastly enhanced in intensity.

Although the result obtained is pretty disappointing but it will form a great platform nonetheless to work on in future research endeavors.

Chapter 6 concludes the research and discusses possible areas of future works.

Chapter2 Literature Review

2.1 Introduction

The literature review has been divided into three major areas of study

a) Polyaniline nanofibers.

b) Raman spectroscopy system.

c) Surface Plasmon Resonance & Surface Enhanced Raman Spectroscopy (SERS).

Although these appear to be different fields of study altogether but this research combines them as surface or interface nano-structures for photonics applications. Polyaniline is a new age polymer used to prepare conductive nanofibers. The preparation techniques, morphology and optical properties are discussed with the help of literature. UV-Visible and Raman spectroscopy techniques are discussed as these could prove useful for characterizing optical properties of nano-structures. These tools again are found useful in literature for investigating optical effects related to nano-structures such as 'surface plasmon resonance effect' and 'SERS'.

2.2 Polyaniline nanofibers: Introduction

Polyaniline (PANI) is among the most extensively studied systems during the past two decades. Polyaniline, resulting from oxidative polymerization of aniline, consists of both reduced (B–NH–B–NH) and oxidized (B–N=Q=N–) repeat units, where B denotes a benzenoid and Q denotes a quinoid ring (Sengupta, 2006). Polyaniline nanofibers, with diameters in the 30–100nm range are described to possess much larger surface to volume ratios.

PANI exhibits unusual combination of color, conductivity and synthetic availability, along with the prospect for practical applications, lends a lasting interest in study of PANI systems. Literature is available for a number of experimental and theoretical investigations dedicated to PANI covering almost all computational levels

such as, molecular mechanics and dynamics (Djurado,2003) including doping mechanism, proton migration, temperature dependence of absorption, and conductivity; Monte Carlo (Schreiber,1996 and Aoki,1998) including interchain electronic transport in disordered systems; Huckel (Wennerstrom,1985) regarding band structure and semi-empirical methods (Libert,1997 and Barta,1998) such as UV/VIS spectra, infra-red and Raman.

The literature review provided here discusses the work done by other authors with due references. Its preparation, reversibility property, fiber structure and physical property characterizations are described in this section.

2.2.1 Preparation of Polyaniline

A variety of methods such as the conventional chemical-polymerization, potentiostatic, galvanostatic and voltammometric electropolymerization processes (Sabatani, 1995 and Liu, 2003) in an aqueous acid have been widely used for the preparation of PANI thin films. Physical methods, including electrospinning (Virji, 2005 and McCall, 1990) and mechanical stretching (Aussawasathien, 2005), were also reported to be capable of fabricating PANI nano-fibers.

2.2.2 Interchangeability of different oxidation states of polyaniline

Huang (2004) et al., has discussed the reversible nature of different oxidation states of PANI. The fully reduced PANI is called leucoemeraldine base (LEB) and is nonconductive; it is a chain of aniline residues with amino nitrogen atoms. Absence of conductivity also is observed in the fully oxidized form, pernigraniline (PNB), with imino nitrogens. The third form, emeraldine base (EB), is semi-oxidized and features alternation of two amino and two imino nitrogen atoms per unit cell (tetramer). These forms can be obtained by appropriate post-polymerization treatment of emeraldine salt of PANI: reduction, oxidation and deprotonation. These changes are accompanied by reversible changes in their color as well making PANI suitable for electrochromic applications. Zhekova (2007) et al., has given a graphical representation of the structure of the three forms.

Li (1998) et al., has explained the reversible effect of polyaniline more comprehensively in terms of the life cycle of reduction and oxidation processes. He describes that oxidation is a two step process taking in excess of 30s while reduction happens more quickly in just about 2-3s.

2.2.3 Morphology of nanofibers

Liu (2003) et al., has explained the growth mechanism of nanofibers as a controlled nucleation growth process. It is pointed out that at a high current density, polymer seeds are firstly deposited on the substrate and then at a lower current density, the polymer nanowire arrays grew from the nucleation sites.

Sadek (2007) et al., has discussed the advantage of nanofibers over conventional film of PANI. Polyaniline nanofibers, with diameters in the 30–100nm range are described to possess much larger surface to volume ratios. This permits easier addition of surface functionality and interaction compared with traditional polyaniline which is highly agglomerated and poorly dispersible in water. Polyaniline nanofibers allow easy diffusion of gas molecules into and out of the film. This provides basis for gas sensing applications of nanostructures PANI (Sengupta, 2006, Debarnot, 2003).

2.2.4 UV-Visible spectroscopy of PANI

There are a number of references on the UV-visible spectroscopy results of polyaniline nanofibers. They appear to agree on the position of absorbance peaks salt and basic form of PANI nanofibers.

(Palys, 2006) et al., has provided two absorption bands at 425nm and 830nm to be characteristic of polaronic charge carriers.

In another reference (Yu, 2007) et al., has reported that the UV–Visible spectrum of the emeraldine salt shows an absorbance maximum at 822nm while emeraldine base spectrum has a strong absorption peak near 600nm.

2.3 Raman spectroscopy system

This is an advanced form of spectroscopy. A cost effective instrumentation is developed in the optical lab. As such a basic understanding of raman spectroscopy, the

scattering mechanism and classical theory that leads to it is properly referenced in this section for better understanding. Also, modern day developments and applications are referenced.

2.3.1 Introduction

Raman spectroscopy, a companion technique to infrared spectroscopy, is capable of giving detailed information about molecular structure and quantitative analysis. It is complementary to infrared spectroscopy in that it provides similar kinds of information about a molecule (i.e., functional groups and structure), but also information for molecules that are not infrared active or are in aqueous solution. Unlike infrared spectroscopy, Raman spectroscopy provides information about totally symmetric molecular vibrations.

2.3.2 The Raman Effect: Scattering mechanism

Raman Effect and the scattering mechanism associated with it, is described in great detail in numerous references (Long, 1977 and Smith, 2005). The essential feature of the mechanism is discussed.

Raman scattering is created by irradiating a sample with a light source at one specific wavelength or color. Today, this monochromatic light source is usually in the form of a laser. In order for this to work, the laser has to possess an energy so as not to be absorbed by the molecule which leads to other effects such as 'fluorescence' and 'phosphorescence'.

This can be an energy that brings the molecule to some virtual state between the ground state and the lowest electronic state. When exciting light source imparts energy to the molecule, on most of the occasions the molecule will jump back down to where it originated from, emitting **Rayleigh** scattering. This scattering is the same wavelength as the light source because

there is no change in excitation energy and thus no change in frequency. When the molecule leaves the virtual state and finishes on the first vibrational level of the ground state, then ΔE is subtracted from the initial energy of the light source equaling $E - \Delta E$.

Since the energy is smaller, the wavelength is longer. This is known as **Stokes** emissions.

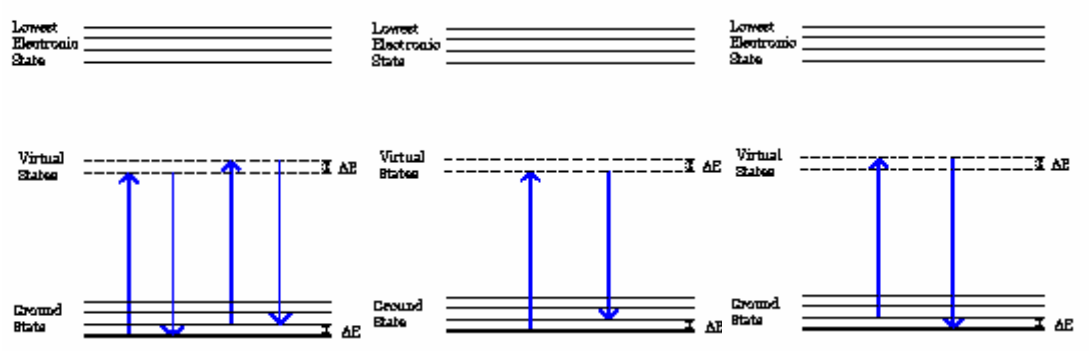

Figure2.1: Molecular scattering: Rayleigh and Raman (Stokes & Anti-Stokes)

If the molecule starts off in the first vibrational level in the ground state when it is irradiated, and the molecule travels back down to the lowest ground state a change in energy is also observed. This is an increase in energy equaling E + ΔE which indicates an emission of a shorter wavelength. This is known as **Anti-Stokes** emissions. In general Rayleigh scattering is 10^6 times more intense than stokes and anti-stokes lines. Stokes lines are usually more intense than anti-Stokes lines. Raman scattering is also about 10^{-5} times the power of the initial light source.

2.3.3 Classical theory of Rayleigh and Raman scattering

Long (1977) et al., has described the interaction of a molecular system with the harmonically oscillating electric field associated with electromagnetic radiation of frequency υ_{ex}. The electric field vector of the exciting source is described by:

$$E = E_o \cos(2\pi\upsilon_{ex}t)$$

where E_0 is the amplitude of the wave. The induced linear dipole moment is a function of electric field and polarizability tensor and has been found to be made of three distinct frequency components: 'Rayleigh' scattering which happens at the same frequency as the light source, 'Stokes' and 'Anti-Stokes' emissions. It has been shown that the magnitude of the Raman Shift is independent of the frequency of the laser.

Every substance has a unique set of allowed vibrational energies, and Raman spectroscopy can be used not only to identify an unknown sample but also can provide information about bond lengths, strengths, and angles.

2.3.4 Introductory Raman instrumentation

The original experiment conducted by Raman, to detect optical inelastic scattering was remarkably simple (Raman, 1928). The introduction of this apparently simple experiment into the sphere of commercial instrumentation had to await the development of sufficiently intense and monochromatic optical sources (i.e. lasers) and more sensitive detectors (e.g. photomultipliers).

2.3.5 Developments in modern day Raman instrumentation

In this Section, some features of the modern Raman system are discussed.

- **CCD (charge-coupled device) based spectrophotometers**

(Pitt, 2005) has described the modern CCD based spectrophotometers in some detail. The original photographic plate used by Raman was able to record a wide spectral range, but the analysis (optical densitometry) and data collection were very slow. CCD arrays subsequently superseded the use of cooled photomultipliers that could only collect one single point of the spectrum at a time.

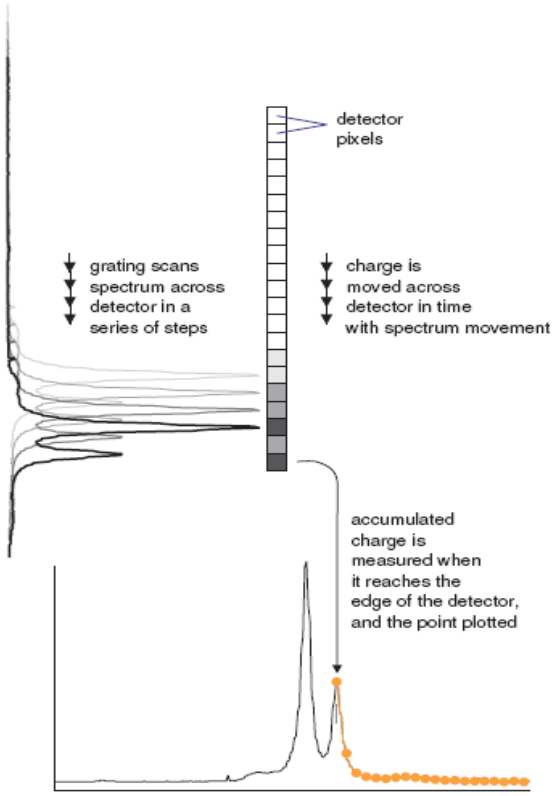

A CCD two-dimensional array comprises a large number of small (10–20mm) individual square silicon

detectors.

Figure 2.2: A CCD array (Pitt, 2005)

A relatively standard method of CCD operation occurs when the image illumination is scanned across the CCD synchronously with the clocking of the active area electrodes, i.e. in time to the readout. This is called time delay and integration (TDI). The synchronous scanning described in Figure is more about driving a spectrum in synchronization with the charge transfer, i.e. actively synchronizing a mechanical motion with the timing of the CCD transfers rather than relying on the image drift due to relative motion.

- **Near the laser line measurement**

Enhancing the ability of the system to exclude Rayleigh scattering has improved the range of Raman spectral frequencies measured, particularly in the region of the frequency of the excitation laser. Initially, filter based systems were able to give results to 4200cm^{-1} from the laser line frequency. This limit has been reduced with further development to approximately 10cm^{-1} for visible wavelength lasers.

- **New multilayer dielectric and holographic dichroic filters**

Initially these were developed for high specification defense applications; but their incorporation for spectroscopy has helped improve band pass and band rejection capabilities (Pitt, 2005).

- **Interfacing to other techniques**

Developing novel fiber optic probes for linking Raman systems into other instrumentation, e.g. scanning electron microscopes (SEM), in vivo biomedical measurement and process control applications has greatly enhanced the sphere of applicability of modern Raman systems(Pitt, 2005).

Incorporation of these sub-systems into the new Raman spectrometers produced a reduction in size, increased robustness, and removed the need for expensive

vibration isolation tables. As a result of the increased optical throughput, lower power lasers (e.g. 1–10mW) could now be used (including small semiconductor devices), further reducing cost and maintenance.

2.3.6 Raman band characterizations

Raman spectroscopy provides characteristic frequencies (in terms of wavenumbers) which are useful in molecular characterization. Raman scattering appears if a bond is polarizable. For this reason, raman is particularly informative about groups like –C-S-,-S-S-, -C-C-, -N=N-, -C=C-. Many excellent texts and tables are available on Raman characterization frequencies (Freeman, 1974 and Dollish, 1974). Long (1977) et al., has provided some characteristic bands which can be used directly for investigation using Raman spectrum alone or a combination of Raman and Infra-red. This is provided in Appendix. Raman is uniquely capable for characterizing many C=C bond stretching vibrations which generally occur near 1640cm^{-1} and are often weak in Infra-red. In fact, when the band is symmetrically substituted, selection rules forbid appearance of any IR band. It is this type of symmetrical vibration with symmetrical charge distribution which is very strong in the Raman.

Information from the references given above, has been specifically utilized to characterize bonds of certain samples being investigated using our Raman setup.

Few other areas of applications of Raman (and/or IR) to characterize bond makings include:

- Aromatic structures. There are several regions of the spectrum with well known absorption characteristics for aromatic structures. This information has again been utilized by us for bond recognition.
- Triple bond and carbon halogen stretchings are again well distinguishable by Raman characteristic frequencies.

2.3.7 Applications of modern Raman spectroscopy

Pitt (2005) et al., has talked in detail about various applications of modern day Raman spectroscopy. Some of these are provided here in table 2.1

Table 2.1: Raman spectroscopy applications

Applications	Examples
Biomedical applications	Detection of cancer: internal (esophagus, colon) Coronary artery atherosclerosis.
Gems and minerals	
Different forms of carbon	Industrial diamond films Diamond-like carbon coatings Carbon fibers Carbon nanotubes and fullerenes
Forensic applications	Inks, questioned documents and fraud Paint and pigments in vehicular acc dent cases Gunshot residues over perhaps handler's clothes. Identification of Drugs/narcotics
Development of Semiconductors	
Pharmaceutical applications	Analysis of tableted and blended materials Detection of polymorphism Detection of inhomogeneities and contaminants

2.4 Surface Plasmon Resonance (SPR) effect

In this section, a remarkable property of metallic nanoparticles is produced as discussed by other authors. Moreover, a biological nanostructure is discussed which is made use as a substrate to fabricate metal nano- structures.

2.4.1 Introduction of biological nano-scale structures

Certain biological systems are known to possess nanometer-scale architectures. In particular, it has been observed that the wings of some cicada species contain arrays of bristle-like structures with a spacing of ca. 100nm and mainly hexagonal symmetry (Watson, 2002).

The cicadas (Cryptympana atrata Fabricius) are either captured locally or bought from specimen factories. The microscopic structures of the cicada wings consist of ordered hexagonal close-packed arrays of pillars with a spacing of approximately 150nm. The height of the pillars is about 400nm and the diameters at the pillar top and bottom are about 100nm and 150nm, respectively. Similar to the cuticle of other insects, the main components of cicada wings consist of an arrangement of highly crystalline chitin nanofibers embedded in a matrix of protein, polyphenols and water, with a small amount of lipid. Crystalline chitin interacts with the protein matrix via hydrogen bonding, which imparts stillness and chemical stability to the structure (Zhang, 2006).

2.4.2 Metallic nano-scale structures

The preparation and optical characterization of precious metal nanoshapes have received considerable attention recently (Aliganga, 2006; Daniel, 2004 and Choi, 2007). This is because of the fundamental scientific questions raised when light interacts with these subwavelength conductors, and because of potential applications of these systems in, for example, medical therapeutics.

2.4.3 Surface Plasmon Resonance mechanism

Although Surface Plasmon Resonance has been widely studied since 70s and 80s of the last century, its use for the development of nano-ooptical sensors and near-field optics makes it a hot topic of research lately and the literature is building very rapidly. (Sherry, 2005 and Klar, 1998) have described surface plasmons, also known as surface plasmon polaritons, as surface electromagnetic waves that propagate parallel along a metal/dielectric interface. Thus when nano-particles/ nano-structures of metals such as Au/Ag interact with an electric field (light) at an incident wavelength it causes resonance (oscillations) which results in strong light scattering and enhancement of local electromagnetic fields causing the appearance of broad, intense surface plasmon bands in the visible range of the spectrum.

The position of the absorption maximum, the bandwidth and the peak height of plasmon resonance frequency depends on the size (Berciaud, 2005) and shape of the

particles (Kelly, 2003), the dielectric constant of the metal (Mulvaney, 1996) and the surrounding medium (Kossyrev, 2005).

Only in the case of well-separated particles in optically thin samples is the response of an N-particle system equal to the N-fold of the individual. In all other cases, inter-particle interactions more or less veil the single-particle properties. Two types of interaction prevail between arrayed metallic nanoparticles: near field coupling (between particles that are close to each other) and far-field dipolar interactions. For near field interacting particles, the plasmon resonance peak is expected to red-shift.

Kreibig (1985) et al., provides theoretical calculations which are restricted to free-electron model from which it is understood that various interactions and processes determine the particle size effect on the plasmon peak positions. Kreibig also provides details of a number of material effects that work together and have been studied by various theoretical models. All/or some of these effects may combine to provide the overall shift in resonance band. These two tables are provided in appendix.

2.4.4 SERS: Surface Enhanced Raman Spectroscopy

Since its first observation by (Fleischmann,1974), the surface enhanced Raman scattering (SERS) technique has evolved as one of the most sensitive spectroscopic tools available in the field of analytical investigation. Detecting the broad range of adsorbate molecules even up to the ultrasensitive, single-molecule limit, SERS shows great promise in overcoming the low-sensitivity problems inherent in Raman spectroscopy (Moskovits, 1985). This method incorporates the analytical advantages of Raman spectroscopy with the additional possibility of detecting very low concentrations.

Two fundamentally different mechanisms dominate in the SERS phenomenon—a classical electromagnetic effect and a ‘‘chemical’’ effect, the main contributor being the former. In the electromagnetic description of SERS, the enhancement is caused by an amplification of the electric field due to the response of the material surface to the incoming wave. Large and spatially confined electromagnetic enhancement effect can be of the order 10^{11}-10^{14} (Xu, 2000).

Chapter 3: Optical Spectroscopy characterization of Polyaniline (PANI) nanofibers

3.1 Introduction

This chapter establishes the optical properties of PANI nanofibers. To meet this aim, a visible spectroscopy setup built in the optical lab is described in section 3.2, along with its components and its operation. Section 3.3 of this chapter discusses a simple reflection experiment carried out to establish the performance of the setup. Section 3.4 then talks about nanometric fibers made of a polymer called polyaniline. It discusses its synthesis by two polymerization techniques and optical properties of the fibers thus made. These properties are eventually proven to be a function of different conditions of doping medium, electrolytic environment and temperature.

3.1.1 What and why of optical spectroscopy

Spectroscopy is basically a study of the interaction between electromagnetic radiation and matter, as a function of wavelength λ. Optical spectroscopy thus refers to the study of interaction of matter with optical radiation such as light in UV or Visible range.

Such an interaction is associated with gain or loss of energy by electrons in the atoms of that material. Study of these interactions, would thus enable understanding of the matter at atomic and electronic scale.

3.2 Visible spectroscopy characterization

Visible spectroscopy is a simple form of spectroscopy. In this section, the visible spectroscopy set-up developed is introduced and discussed. Important components of the setup are also discussed in detail. A halogen light source was used s a source for visible light. This setup was further improved into a UV-Visible spectroscopy setup by using a light source from Micropack Inc. which had a deuterium light source as well.

3.2.1 Visible spectroscopy set-up

For the purpose of obtaining a visible spectrum, a visible spectroscopy setup was configured. A visible spectrum is obtained over a wavelength range of 400nm to 700nm. This setup is capable of providing results for multiple kinds of spectroscopy such as absorption, transmission and reflection.

The setup is shown in figure 3.1 and includes a Nikon inverted microscope (TE 2000U) and a personal computer (PC) attached to an Ocean-Optics spectrometer which is a light detection system.

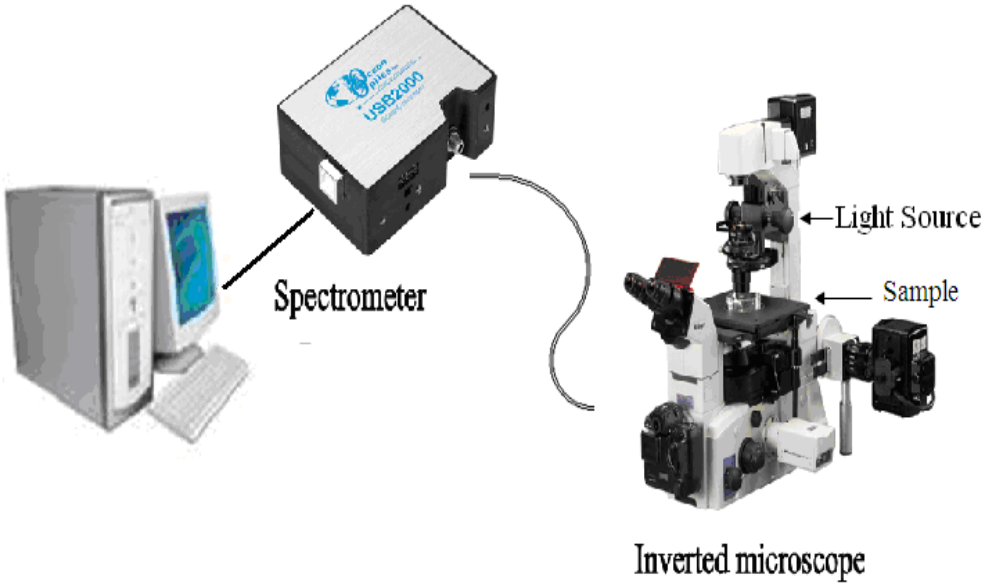

Figure 3.1: The UV-Visible spectroscopy characterization setup

3.2.2 Important components of the detection system

a) The hardware: USB2000 spectrometer

The USB2000 spectrometer shown in figure 3.2 was purchased from Ocean Optics Inc. and comes with a fiber-optic input. The USB2000 miniature spectrometer is a small-footprint, plug-and-play spectrometer.

The spectrometer has smart features such as automatic capability to read the wavelength calibration coefficients of the spectrometer when first configured and

configures the operating software as well. It also has a USB-to-PC interface. It doesn't have any external power requirements and is powered by PC itself.

Figure 3.2: A USB2000 spectrometer (courtesy Ocean Optics Inc.)

It is UV-enhanced and equipped with a 300µm diameter fiber, 600 line/mm grating blazed at 300nm and a 1000µm x 100µm slit. This combination of components provides an optical resolution of approximately 1.33nm FWHM (full width at half maximum). This is an equivalent resolution of 83cm^{-1} wavenumbers. Resolution could be improved, with the use of a smaller slit and/or a finer grating but at the sacrifice of sensitivity. Slits down to 5 µm and gratings up to 1800 lines/mm are available from the manufacturer. Note that the grating blaze wavelength must match the laser wavelength closely if these finer gratings are used. If a 10µm slit and 1800 lines/mm grating is used, the resolution could be improved to 0.30nm FWHM, which is an equivalent resolution of 19cm^{-1}. The drawback would be an increase in cost and poorer sensitivity.

The spectrometer uses a 2048-pixel CCD-detector array. Each pixel has a size of 14µm x 200µm with pixel well depth ~62,500 electrons. It has a signal-to-noise ratio of 250:1 (at full signal) and an A/D resolution of 12 bit. It can be used to detect Raman scattering as well. Due to the recent development of silicon CCD cameras, the CCD sensor has replaced the single channel detector, photomultiplier tube (PMT) and avalanche photodiodes (APD), as a multichannel photon detector in the spectrometer. The CCD array behaves much like a photographic film, in the sense that the array

integrates incident photons over time. Thus, the longer the exposure, the more faint the light can be detected. Typical integration time of a CCD spectrograph is less than 30s. A CCD sensor requires lesser integration time compared to earlier technologies because it allows spectrum multiplexing (Pitt, 2005). It can detect radiation from 200nm to 1100nm but for our purposes it is configured to be most efficient in the range of 450nm to 700nm.

b) The software: 'Spectra Suite' from Ocean Optics

The Ocean Optics spectrometer software allows integration times to be varied from 3ms to 65s; for most samples, integration times of between 5s and 60s are required. To obtain a raman spectrum and because of relative weakness of the Raman signal in comparison to pixel noise, a dark spectrum (with laser light blocked) must be subtracted from the overall signal. The 'spectra-suite' explicitly allows for dark spectrum subtraction. The dark spectrum must be collected using the same integration time as the spectrum. Also a reference spectrum is advisable to be taken as it is used for calibration of the hardware. The software is configured automatically as the spectrometer reads wavelength calibration data on its own. Obtained spectrum is thus doesn't need to be corrected for any wavelength variation in the response of the CCD detector.

For raman measurements the common unit of wavelength measurement is wavenumbers (cm^{-1}) which gives the shift of raman signal from the rayleigh wavelength. The software is enabled to make the change from wavelength to wavenumber. An example to explain the relationship between wavelength and wavenumber could be that of a silicon which shows strong raman peak at $520cm^{-1}$. The relationship between absolute wavenumber (ν') and wavelength (λ) is: $1/\lambda = \nu'$. The normal relationship between wavelength and frequency also holds: $1/\lambda = \nu/c$; where c is the velocity of light (2.99793×10^{10}cm/s), ν is the frequency of the scattered light in units of s^{-1} (Hz) and the wavelength λ is in nm (Pitt, 2005).

The dynamic range (or the range of suitable operation) for the available spectrometer could now be worked out making use of the knowledge of relationship between wavenumber and wavelength. For an excitation laser light of wavelength equal

to 532nm, the wavenumber corresponds to 18797cm^{-1}. The raman shift would thus be 0cm^{-1}. The wavelength range for the spectrometer is known to be 450 to 700nm, and is provided in section 3.2.2 (a). The dynamic range in terms of wavenumber would be for the spectrometer can now be worked out. 450nm corresponds to 16574cm^{-1}, which makes the raman shift equal to -3425cm^{-1}, while 700nm would correspond to 4511 cm^{-1} .

3.2.3 Operation of the spectroscopy setup

Optical characterization can be carried out by placing the sample on the x-y-z translational stage of an inverted microscope. An inverted microscope has a light source above the sample such that light is incident normal to the sample surface.

The detection microscope objective is underneath the sample translational stage and its height from the sample can be adjusted such that the sample lies at the focal point of the objective. Objective of required magnification and numerical aperture can be put in place.

Light is transmitted through the sample and collected by objective. The transmitted light is captured in the far-field, whereby the collection and spectral measurement take place. The objective causes the emerging light to be imaged into the output port of the microscope and onto the open end of the optical fiber coupled to the spectrometer system. In this manner, a transmission spectrum can be obtained using an inverted microscope.

If a spectrum other than transmission such as reflection or absorbance is desired for a sample, experimenter does not need to make any changes in setup and configure it for reflection which would make experimentation a complex affair. The software ‘spectra-suite’ described in section 3.2.2 is capable of providing these spectra by itself. The experimenter just needs to make some changes in the software settings making it to use an in-built mathematical function for the relationship between ‘reflection’, ‘absorbance’ and ‘transmission’.

This allows minimum handling of delicate samples and also achieves multiple types of spectroscopy measurements using a single setting.

3.3 Validation of spectroscopy setup

This section describes a preliminary experiment carried out to establish the operation of developed visible spectroscopy system. The sample used for this purpose is a 'thin film' material based on glass substrate. In this work, visible spectrum confirming reflectivity of the sample is obtained, in accordance with the simulations by (Thach, 2006).

3.3.1 Sample description

Figure 3.3 shows a schematic diagram of 'thin film' sample. It is made of a layer of tantalum pentoxide (RI=2.10) which has higher refractive-index compared to the substrate (glass, RI=1.5). The thickness of the film is taken to be approximately 130nm.

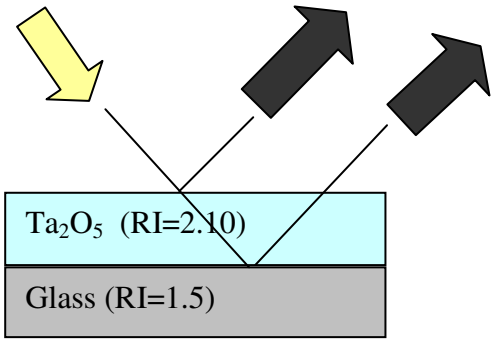

Figure 3.3: A thin film high reflection stack

3.3.2 Result

Looking at the 'spectrograph' window in figure 3.4, the region of high reflection can be observed. There are two important observations that can be made from the spectrograph result:

1) The overall reflection is high within a broadband stretching from approximately 450nm to 650nm beyond which it decreases on both ends of the spectrum with additional system noise.

2) The reflectivity is found to be maximum in the vicinity of 525nm being approximately 40%.

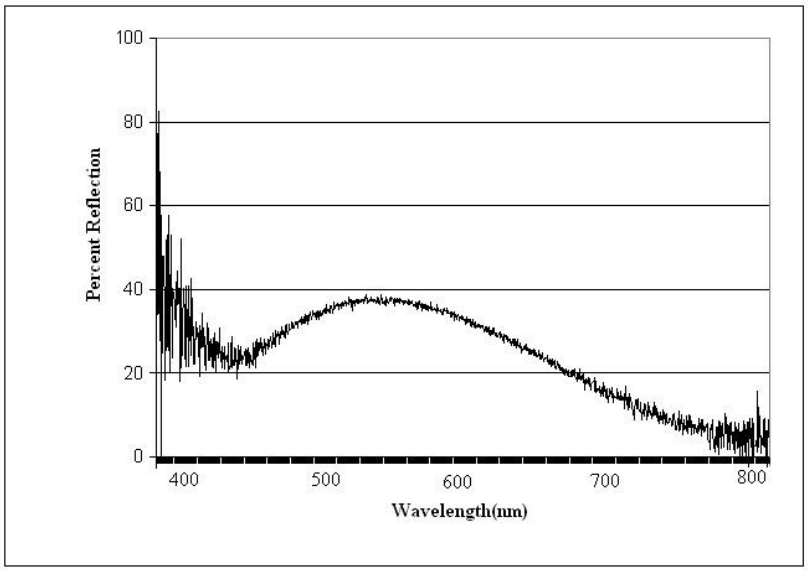

Figure 3.4: Reflection spectrum obtained for a 'thin film' high reflection coating mirror

3.3.3 Discussion

Since a white light source has been used for this experiment, the region of observation is most suitable within the 400nm to 700nm range. High reflection capability has been demonstrated for a thin film using a simple optical spectroscopy technique. The thickness of tantalum pentoxide layer is chosen in such a manner that it is a quarter-wave thickness ($\lambda/4$). This means that the wavefronts reflected from the surface of the two layers interfere to produce maximum reflectivity at λ near 520nm. Thus, by choosing materials of appropriate refractive indices and thicknesses, more efficient reflector than glass can be produced.

The system noise that is observed on both ends of visible spectrum defines the region of normal operation for a CCD based light detection system. It appears that the region of operation of the spectrometer is limited to the range 450-700nm. The makers 'Ocean Optics Inc' have defined this range as the 'dynamic range' for any

spectrometer. The main contributors to this dark signal being the system electronics noise. (Ocean Optics website)

3.4 UV-Visible spectroscopy characterization of PANI nanofibers

After studying the performance of visible spectroscopy system through previous experiment, it can now be made use to study optical properties of polyaniline nanofibers but first an understanding of PANI nanofibers is produced. PANI nanofibers were prepared by two different techniques and deposited as thin films on substrates. Experiments were carried out on prepared films to characterize them for their electrical and optical properties, under different conditions of electrolytic environment, oxidizing conditions and temperature.

3.4.1 Introduction to PANI nanofibers

Polyaniline (PANI) in the form of nanofibers has been synthesized as part of the research. PANI can switch reversibly between the electrical conducting and insulating forms through a doping and undoping process (Kane-Maguire, 1999). It is found to exhibit color changes as the oxidation condition changes. Color is found to change from transparent (leucoemeraldine) to yellow/green (emeraldine) and eventually to blue/black (pernigraniline) (Chen, 1996). The present investigation, establishes the relationship between different doping levels according to the potentials applied, on electrical and optical properties of polyaniline.

Two methods, chemical and electro-chemical polymerization techniques were used for polymerization of aniline to form polyaniline. Preparation by the two techniques is discussed along with the experiments done on the films.

3.4.2 Synthesis of PANI nanofibers by chemical polymerization technique

Chemical polymerization is first of the two techniques employed for preparing PANI nanofibers. After obtaining the nanofiber films, these were tested for their electrical and optical properties.

3.4.2.1 Sample preparation

Polyaniline was first synthesized using the chemical polymerization technique. In this process, 0.3M concentration of aniline monomer was rapidly added into 1.0M concentration of camphorsulfonic acid (CSA) solution although a great variety of other dopant acids can be used, including: hydrochloric, sulphuric, nitric, phosphoric, perchloric, acetic, formic, tartaric, camphorsulfonic, methylsulfonic, ethylsulfonic, and 4-toluenesulfonic acid among others (Huang, 2004). Adding the two in given proportions started the oxidation process. To enhance the oxidation process, ammonium-persulfate $(NH_4)_2S_2O_8$ (an oxidant) was added to the mixture and was allowed to react further overnight. Resultant solution was the emeraldine salt form of polyaniline.

The initially prepared CSA-doped polyaniline was washed with 0.1M NH_4OH to convert it to emeraldine base and was called dedoped PANI (Huang, 2004). The undoped (dedoped) polyaniline film was obtained by casting a drop on a glass slide. There were three such films prepared. The films were left to dry overnight. For protonic doping, films were dipped in different concentrations of HCl solution (viz. 1%, 5% and 10% w/w, respectively) and were left to dry overnight.

3.4.2.2 Result and discussion of chemical polymerization

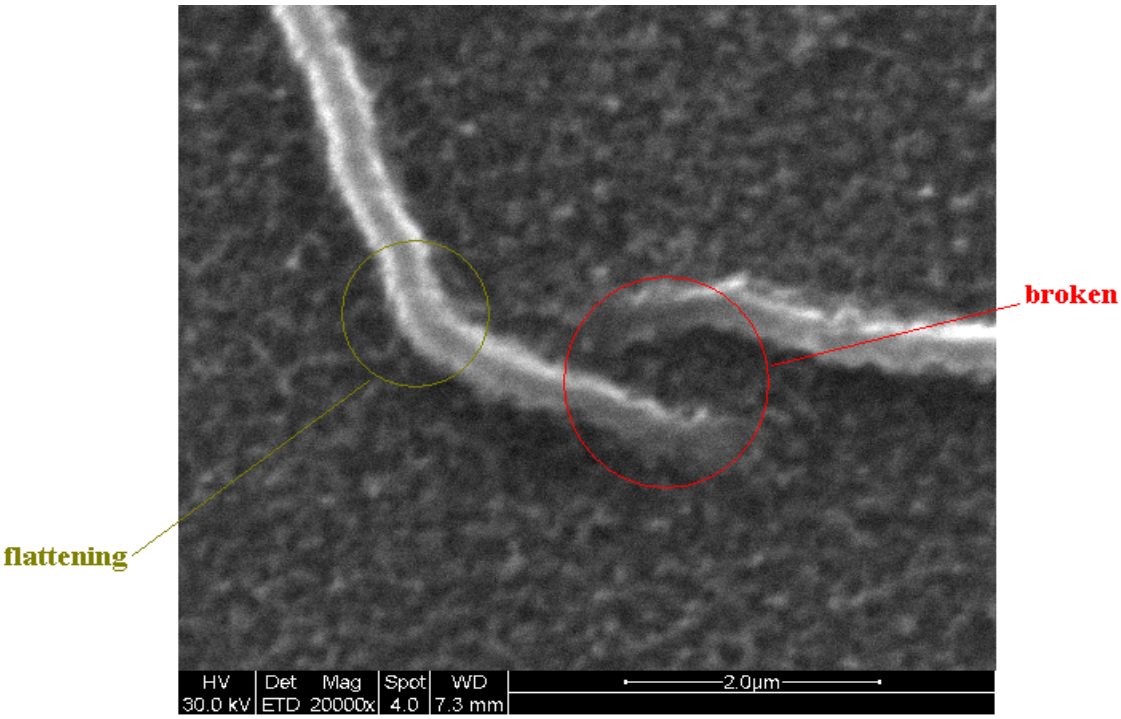

Figure 3.5: SEM image of PANI nanofiber obtained by chemical polymerization

The Scanning Electron Microscopy (SEM) image in figure 3.5 of completely dried film of PANI was obtained to establish the quality of nanofibric film. The image revealed that nanofibers appeared to be highly agglomerated, fused, flattened and broken. It was also revealed that irregular nanostructures were prevalent. This could be lot to do with the process of drop-casting on glass slide which can cause unordered and uneven distribution of polyaniline. It can be concluded that this process did not give ordered and even structures to nanofibers.

It can be noted here that PANI nanofibers are redoped with a different acid (HCl) as compared to the initial synthesis where CSA was used. The study by (Sarno, 2005) et al., further confirms this process.

3.4.2.3 Electrical property characterization: conductivity dependence on doping

Having obtained films of nanofibers doped with different concentrations of dopant medium, they were tested for the effect of variable doping on the electrical conductivity. A 'four point probe' method was used for this purpose.

- **A four point probe equipment description**

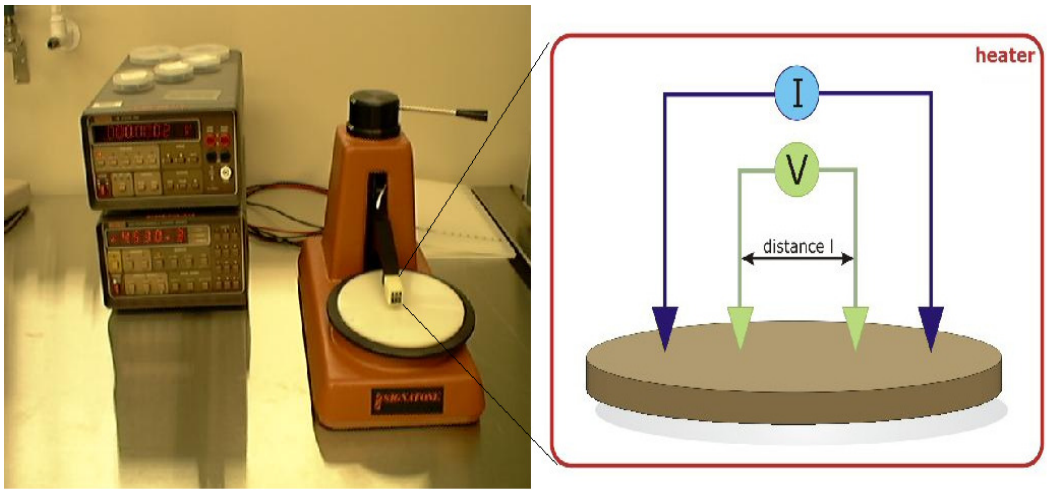

Figure 3.6: A four point probe setup, depicting the functioning of probe points, distance between probe points being 1mm.

The four-point probe station consists of a SIGNATONE probe station (four probe tips), an ampere meter (FLUKE8010A), a DC current source (HP6181C), and a voltmeter (KEITHLY195). This set up can measure resistivity of thin film material, as well as diffusion layers. The four probes are arranged in a linear fashion, where two outer probes are connected to a current supply, and the inner probes to a voltage meter as shown in the figure 3.6. As current flows between the outer probes, the voltage drop across the inner probes was measured. Applied current was varied in steps and the corresponding voltage was measured to determine whether polyaniline possesses ohmic or rectifying contacts (Sengupta, 2006). The relationship of the current and voltage values is dependent on the resistivity of the material under test, and the geometrical characteristics of the probe as per follows:

$$\rho = 2\pi S(V / I), \qquad (3.1)$$

where S is the probe spacing (mm), which was kept constant, I is the measured current in mA, and the corresponding voltage, V, was measured in mV. Conductivity σ can be calculated using the relationship:

$$\sigma = 1/\rho, \qquad (3.2)$$

3.4.2.4 Result and discussion of electrical characterization

Current and voltage were varied for a range of values. The linear relationship of current and voltage in Figure 3.7 clearly suggests that PANI possesses ohmic properties. Current was found to be directly proportional for a long range of values and as such breakdown values couldn't be ascertained.

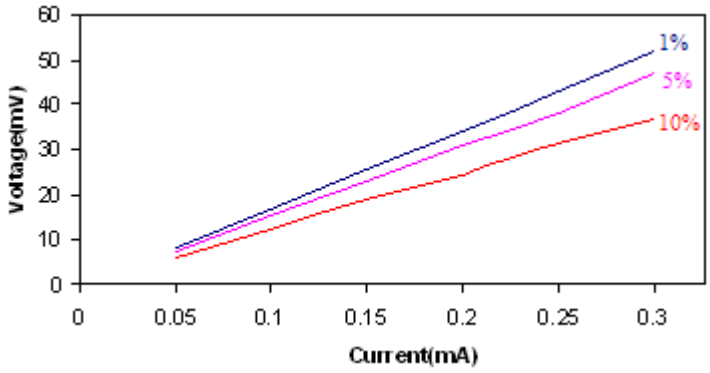

Figure3.7: I-V characteristics of PANI films doped to different extents

The electrical conductivity calculated using Equation 3.1 & 3.2 is given in Figure 3.8 which gives relationship between the doping concentration and conductivity, indicating increase in conductivity with the increase in doping concentration. Conductivity is found to be in low mS range and this is acceptable considering the low

concentration (%w/w) of doping agent used. The conductivity is bound to increase with doping concentration as the conductivity curve suggests.

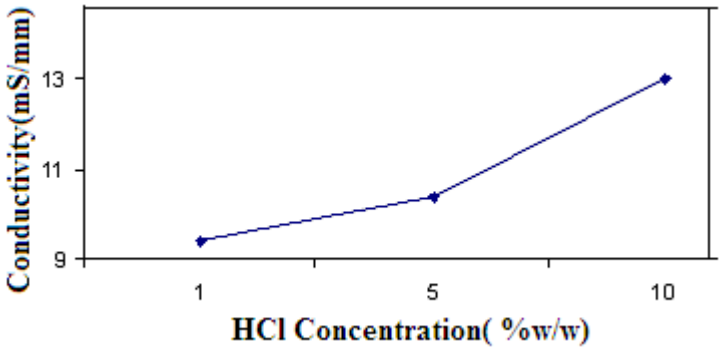

Figure 3.8: Doping concentration vs conductivity curve for PANI films

3.4.2.5 Optical characterization: transmission spectroscopy of PANI

Having established the conductivity dependence of PANI films on doping levels, they were next tested for their optical properties. Optical characterization of the polyaniline films was obtained using UV-Visible spectroscopy. The transmission spectrum is acquired using the Ocean-Optics USB-2000 spectrometer attached to an output port of an inverted microscope (courtesy Nikon Corporation). The setup has been described in detail in section 3.2.

3.4.2.6 Result and discussion of optical properties

The initially prepared CSA-doped polyaniline fiber was dispersed in de-ionized (DI) water. It was green in color and became violet-blue upon washing with substantial amounts of 0.1M NH_4OH. This is an indication of conversion of PANI salt to basic form due to its deprotonation (reduction) which is called dedoped PANI (Sengupta, 2006). The conductive polymers such as polyaniline are highly colored because their (π- π^*) energy gap falls within the visible region. Those wavelengths which are not absorbed but transmitted, result in the observed color (Sengupta, 2006). The optical spectrum obtained before and after the deprotonation process clearly verifies this change. The leftmost peak (~420nm) in the transmission spectrum shown

in Figure 3.9 is indicative of the emeraldine base (dedoped) form of PANI which is violet-blue in appearance. Dipping the emeraldine base cast film in 1% aqueous solution of HCl, resulted in return of the characteristic green color of metallic emeraldine hydrochloride. This is indicated by the shift in transmission peak to ~500nm. Thin films of emeraldine base dipped in different concentration of HCl (1%, 5%, 10% w/w) suggests the expected red-shift in peaks which is caused due to gradually increasing protonation to emeraldine salt. Doping with different concentrations caused protonation in quinone di-imine units to different extents (Sarno, 2006).

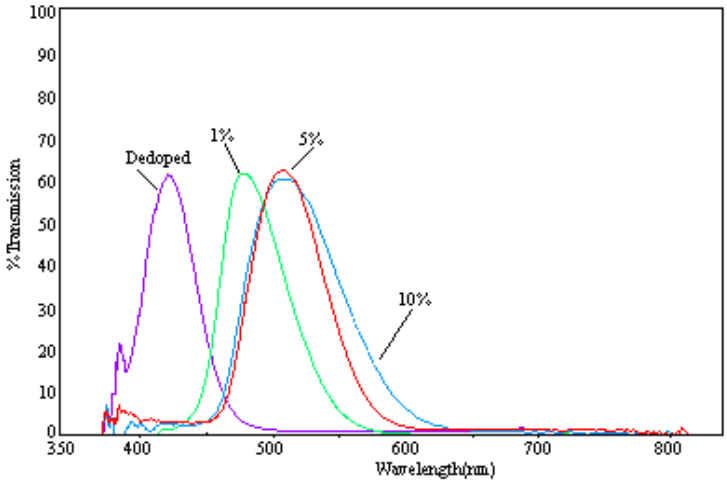

Figure 3.9: Transmission spectra of chemically doped PANI samples

3.4.3 PANI synthesis by electro-chemical polymerization technique

Electro-polymerization of PANI nanofibers is considered a significant way of producing ordered PANI nanofibers. PANI nanofibers were fabricated on a transparent conductive glass (indium tin oxide, ITO) substrate through a controlled potentiostatic electropolymerization process. Large areas of nanofibers grew vertically on the substrate without using any templates.

There were basically three sets of experiments carried out to investigate the optical properties of polyaniline using nearly the same experimental setups but carried

out under different conditions of voltages (constant voltage or multi-step constant voltage), different temperatures and under different electrolytic environments (acidic and neutral medium).

3.4.3.1 Sample preparation

PANI nanofibers were prepared by a controlled potentiostatic electropolymerization process on a conventional three-electrode system. The electrolytic cell consisted of a piece of ITO glass sheet (sheet resistance<70Ω/square, 2×2 cm^2) which was used as the working electrode and a platinum sheet (2×2 cm^2) served as the counter-electrode. The distance between the working electrode and counter-electrode was ~3 cm (Yu, 2007). Anodic deposition was controlled by an electrochemical station, in an electrolytic solution of 1.0 M HCl containing 0.3 M aniline monomer. The electrolyte solution was prepared in DI water at room temperature. A mechanical stirrer was put in the cell to continuously stir the solution during polymerization, to ensure even and ordered deposition of the polymer on the substrate. A DC power source to supply the needed potential and a digital multimeter to observe and record the current flow were used.

The polymerization is first carried out at a higher voltage (0.75V in the first case) for 5mins and then at a relatively lower voltage (0.65V) for 25mins. Using this methodology, four samples were prepared which are discussed as experiment 1 in section 3.4.3.3.

3.4.3.2 Result and discussion of electrochemical polymerization

It is known from a previous paper by Yu (2007) et al., that the slower the growth rate, the more ordered and dense the structures that can be obtained. When a controlled gradually decreased voltage was applied, the morphologies of the PANI films were found to significantly change. The optimized electropolymerization conditions were investigated for depositing PANI nanofibers in a controlled multi-step constant voltage process. Yu has explained the growth mechanism as a controlled nucleation and growth process. It was pointed out that at a high current density, polymer seeds are firstly deposited on the substrate and then at a lower current density,

the polymer nanowire arrays grew from the nucleation sites. These findings were verified from our experimental study and the SEM images shown in Figure 3.10.

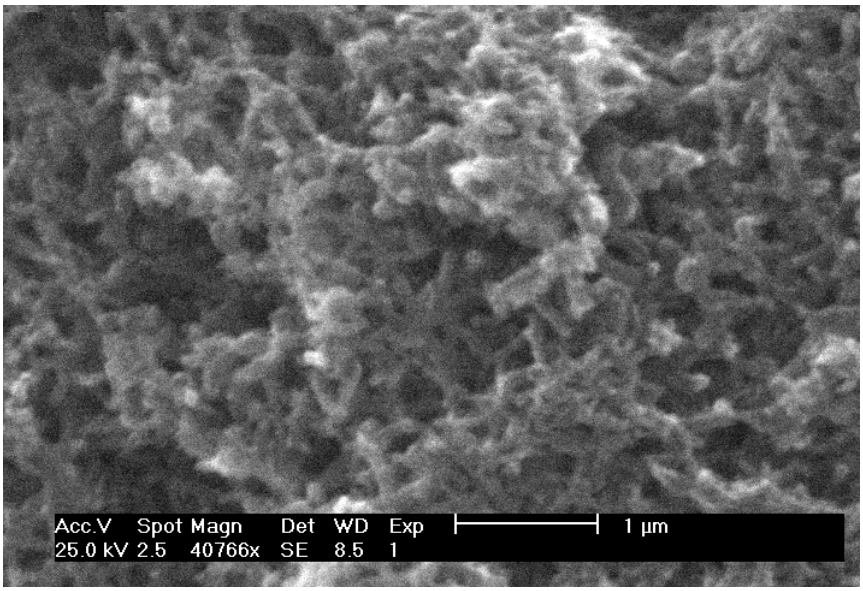

Figure 3.10: SEM image of PANI nanofibers

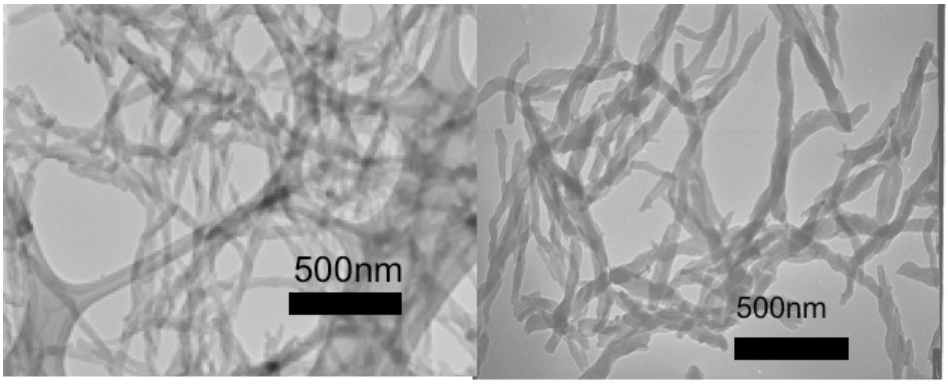

Figure 3.11: TEM images of PANI nanofibers

Transmission Electron Microscopy (TEM) images obtained by our collaborators at UCLA, USA are shown in figure 3.11. These images reveal that the polyaniline nanofiber layers consist of a large quantity of wirelike nanostructures. The

average diameter of the polyaniline nanofibers is approximately 30nm when HCl is used as a dopant agent during synthesis and about 50nm when CSA is used as the dopant agent, with lengths up to several micrometers. The diameter of the nanofibers is strongly related to the dopant acid used in the polymerization process (Sadek, 2007). Examination of several regions on the sample revealed mats of interwoven and twisted nanofibers. Though fibers were the dominant morphology, they were typically accompanied by some small, non-fibrous particles.

Comparing the images from SEM and TEM, it can be suggested that SEM may not be the best tool to observe nanofibers.

In this context a comparison of SEM and TEM technique has been provided.

Table 3.1: Comparison of SEM and TEM

Characteristics of TEM:	**Characteristics of SEM:**
• A beam of electrons replaces a beam of light, and electromagnets replace glass lenses.	• Lenses form the electron beam into a finely focused probe.
• Image is formed by deflection of electrons that pass through the specimen in a vacuum	• Generates the image of the surface of a specimen, by analyzing electrons emitted from a specimen
• Darker areas of the image show that the sample is thicker or more dense in these areas	• Can produce an image that is a good representation of a three-dimensional specimen.
• A magnification of 300,000 times can be routinely obtained for many materials	• Specimens must be coated with a layer of conductive heavy metal (i.e. gold or palladium)
• The microscope uses a 40 to 100 kilovolt electric charge to generate the electron beam	• A magnification of 100,000 times can be achieved for certain specimens

3.4.3.3 Experiment 1: Preparation of PANI in a controlled voltage and acidic environment

Polyaniline was synthesized using the described setup and four such depositions were carried out, each under a different set of conditions as listed in table 3.1. Figures in brackets give the time for which voltage was kept constant. The optical result is provided in figure 3.11.

Table 3.2: The four PANI samples prepared under the given conditions

Samples Prepared	V_1 (time, min)	V_2 (time, min)	Temperature (°C)
1	0.75V(5)	0.65V(25)	25(room)
2	0.65V(5)	0.55V(95)	25(room)
3	0.75V(5)	0.65V(5)	0(zero)
4	0.65V(5)	0.55V(95)	0(zero)

3.4.3.4 Result and discussion of experiment 1

Figure 3.12 gives the spectra and compares the curves obtained for PANI deposited on an ITO under the sets of conditions given in Table 3.1. The two absorbance bands at approximately 420nm and 825nm are probably characteristic of polaronic charge carriers for PANI (Palys, 2006), as discussed in literature review. The increased absorbance is indicative of the controlled growth process. Also, changing the temperature from room temperature to close to the temperature of ice bath keeping the polymerizing potential constant is also found to increase the absorbance, justifying the fact that the temperature does influence the formation of nanofibers.

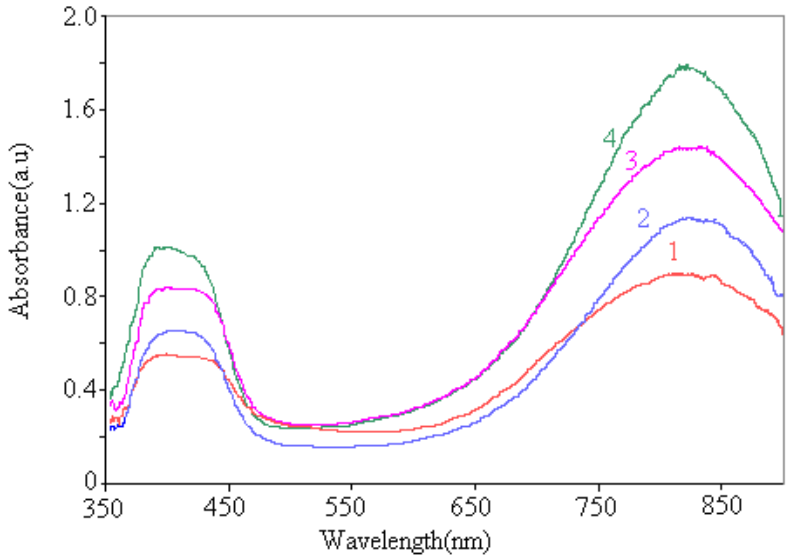

Figure 3.12: Absorption spectra of PANI deposited on ITO glass substrate (experiment1)

3.4.3.5 Experiment 2: Effect on PANI due to gradually increasing controlled voltage in acidic medium

One of the four prepared PANI samples (no.2) was taken and tested in the electrolytic cell to observe the effect of increasing voltage on it. It was expected that the increase of potential in the presence of doping agent works to oxidize the sample while a decrease would cause a reduction reaction to take place.

The electrolyte this time was taken as 1.0M HCl. There was no need to add aniline, as already prepared PANI film was tested for the effect of doping only. An electrolytic cell similar to the one for polymerization was used for this purpose. The ITO based PANI sample was placed at a distance of about 3cm from platinum electrode. The stirrer was put at a safe distance from the sample so that it doesn't damage the sample by hitting it.

In this case, the voltage was gradually increased in steps of 0.05V over a range of 0.40V to 1.25V. It was observed that the voltage couldn't be increased as it

started to bleach away the polyaniline from its substrate. The process of voltage variation is better understood by looking at figure 3.13.

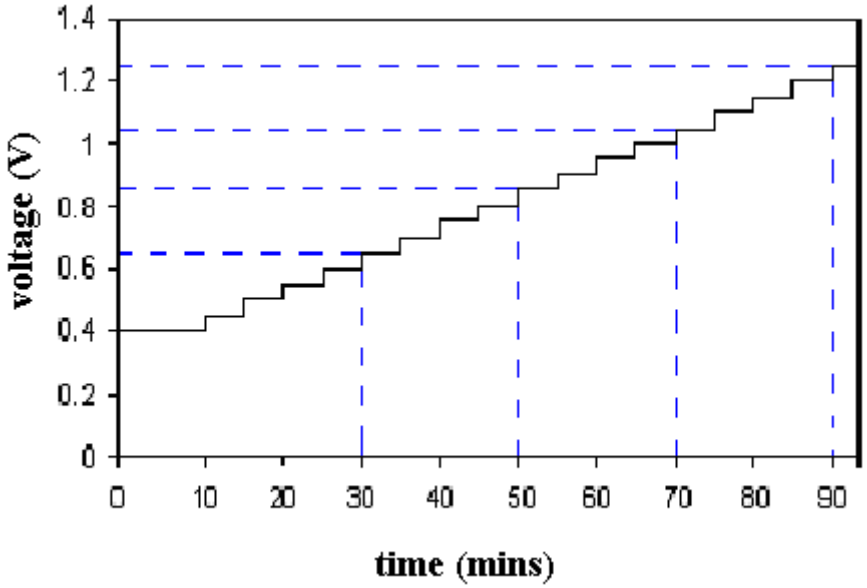

Figure 3.13: Time-voltage curve for sample 2 in HCl solution

Each voltage step was held constant for time span of 5mins. The dotted lines represent the interval at which sample was taken out and its visible spectrum taken. Its spectrum was obtained and the process continued in a similar way. The sample was thus observed at four time intervals. This procedure produced samples doped by increasing amounts of acid.

3.4.3.6 Result and discussion of optical properties of experiment 2

Figure 3.14 gives the optical spectra for a PANI sample (no.2) under the influence of gradually increasing oxidising potential in an acidic medium. The absorbance image describes the increased absorbance taking place with increasing applied voltage. This can be attributed to the fact that as the polymerizing voltage increases, PANI becomes more oxidised (protonated) in the presence of doping medium and changes state as well as color and absorbs more light.

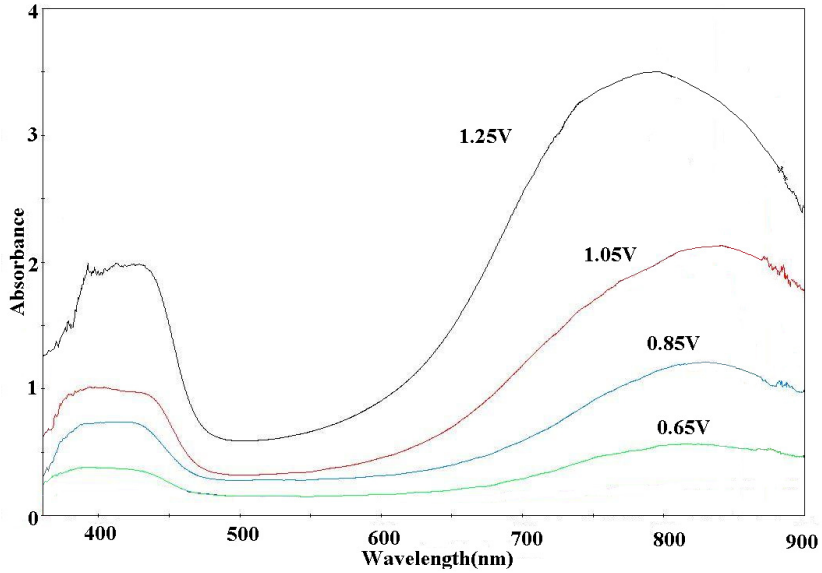

Figure 3.14: UV-Visible absorption spectra of sample 2 (experiment 2)

3.4.3.7 Experiment 3: Influence of voltage in a neutral medium

In this experiment, the experimental conditions were again altered. The highly acidic HCl solution was replaced by a neutral 1.0M NaCl salt solution as the electrolyte in the cell. The effect of oxidising voltage under the influence of neutral electrolytic solution, on the PANI film was observed. It was observed that the voltage this time could be made higher than previous experiment without deteriorating the sample. The voltage was gradually increased from 0.5V to 10.5V, in steps of 0.05V, each held constant for a period of 5mins. The change in color appeared to be taking place much slower this time compared to experiment 2 when acidic electrolyte was used. The optical spectrum is provided in figure 3.15.

3.4.3.8 Result and discussion of experiment 3

The effect of increasing voltage is pretty evident even in the case of a neutral electrolytic solution such as NaCl where higher potentials could be reached due to the neutral nature of the electrolyte. It is understood that the neutral nature of electrolyte caused oxidation reaction to proceed slower than under the acidic electrolytic condition.

Also, the color change process was found to progress slower than before which can again be related to slower rate of oxidation in the present case.

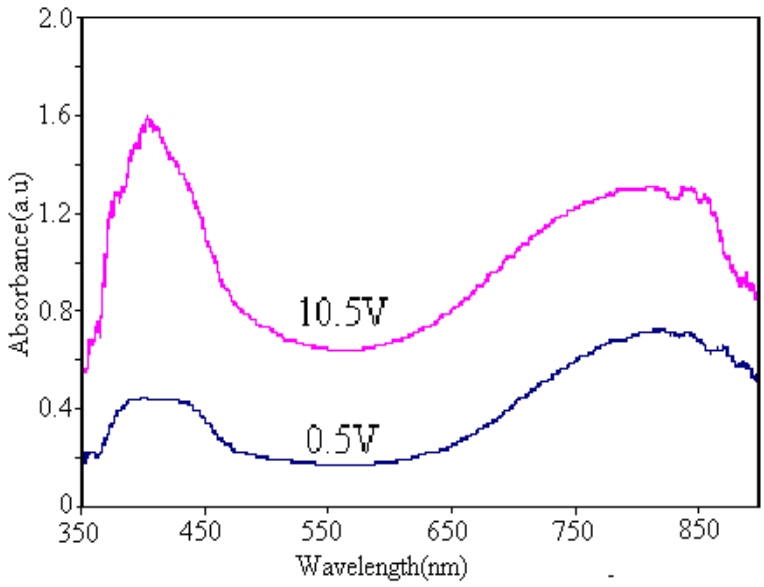

Figure 3.15: Absorbance spectra for PANI in NaCl electrolyte (experiment 3)

The absorbance image is shown in Figure 3.15. This process is also found to be reversible i.e. reducing the voltage made PANI film more transparent thus reducing absorbance.

3.5 Conclusions

Through the present investigations, it has been demonstrated that the optical and conductive properties of polyaniline nanofibers is dependent on doping variables. Inter-conversion of polyaniline (from salt to base and vice-versa) was carried out and was verified by the optical results obtained. The protonation of the PANI base results in a substantial increase in conductivity. Moreover, it can be concluded that doping (and/or undoping) process can be controlled by potentials applied during the polymerization process itself which is confirmed by the optical spectrum provided for each case. Increase in this potential led to more oxidation while a decrease caused reduction process. Also temperature was found to have significant effect on the

polymerization process as shown by the change in absorbance with the change in temperature conditions of the electrolytic cell.

The interchangeability of color property of PANI film can be made use in the development of electrochromic devices and windows.

Chapter 4: A custom-built portable Raman system

4.1 Introduction

Having established UV-Visible spectroscopy as a useful means of optical characterization in chapter 3, let us move one step ahead and establish yet another powerful spectroscopic measurement technique namely Raman spectroscopy. Both techniques will be used in chapter 5 to investigate optical properties of another set of nanostructures.

A portable and compact Raman spectroscopy system developed in the optical lab is described in this chapter. This chapter describes the instrument, its different components and operation of the system. Later in the chapter, system's operation is validated through experimentation carried out on a few samples.

4.2 Instrument description

A Raman system as compared to UV-Visible has a difficult design and requires complex networking of components. Some of the important components of Raman include: a laser light source, set of optical filters to suitably filter different wavelengths of light, beam splitter or a dichroic mirror and a detection system such as a PMT or CCD based detector. The optical components such as filters, beamsplitter and optical collimator has been obtained from the optics shop of 'Lastek Inc.', while the spectrometer is obtained from 'Ocean Optics Inc'

The designed Raman system uses a low cost CCD based spectrometer as the detection system. Being low cost, this spectrometer withholds the objective of this research to build a low cost Raman system. A T-shaped metal assembly ("T") has especially been made to house all the optical components comprising Raman. It has suitable input/output ports for incoming/outgoing laser beams and also has a port for sampling stage. A schematic layout of the whole system is shown in figure 4.1 together with "T" at its heart. The diagram also shows the passage of light as it traverses through the assembly. The operation of the system is described in section 4.3.

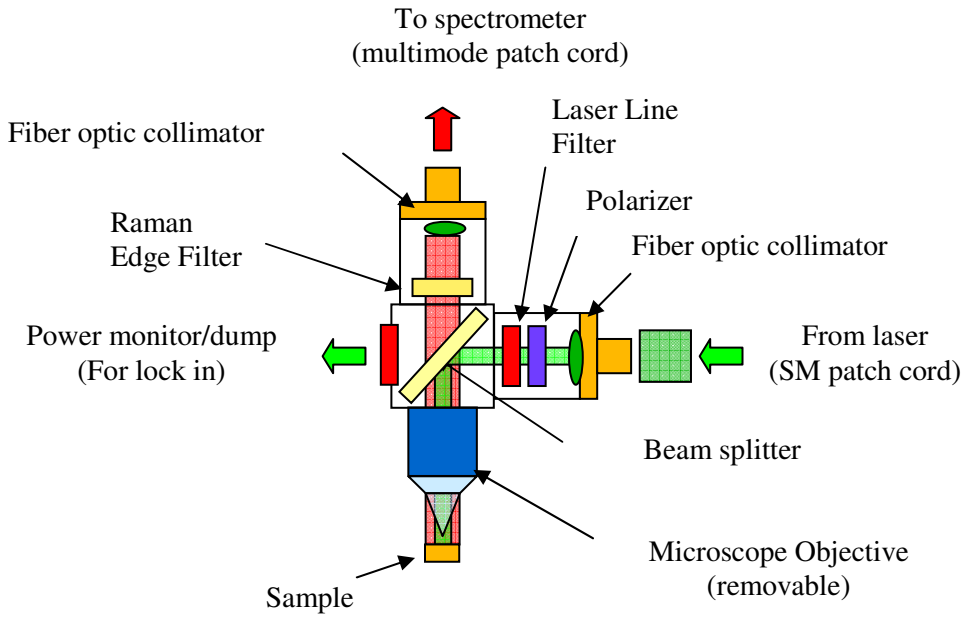

Figure 4.1: A schematic diagram of the developed Raman system

4.2.1 The "T"

This is the central component of the Raman system. The Raman system has been designed in such a way that all the optical components are assembled together in a T-shaped metal assembly made of steel rather than conventionally aligning them individually on a standard optical bench. The idea behind this is to keep human interference to minimum once the optical components are assembled and sealed. This would also protect optical components from dirt and humidity. . It is basically made up of three components and a microscope objective that attach with each other according to figure 4.2 to give it a T shape. It is designed in such a manner to possess proper input and output ports to couple with the laser source, sampling stage and the detection system. The components are listed as:

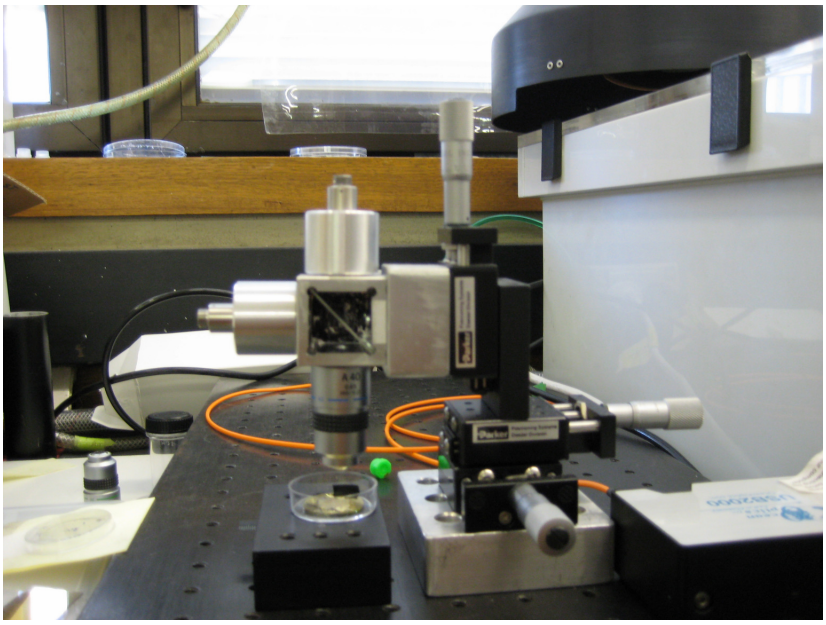

Figure 4.2: The Raman "T" assembly fitted on a translational stage

a) The "Cube"

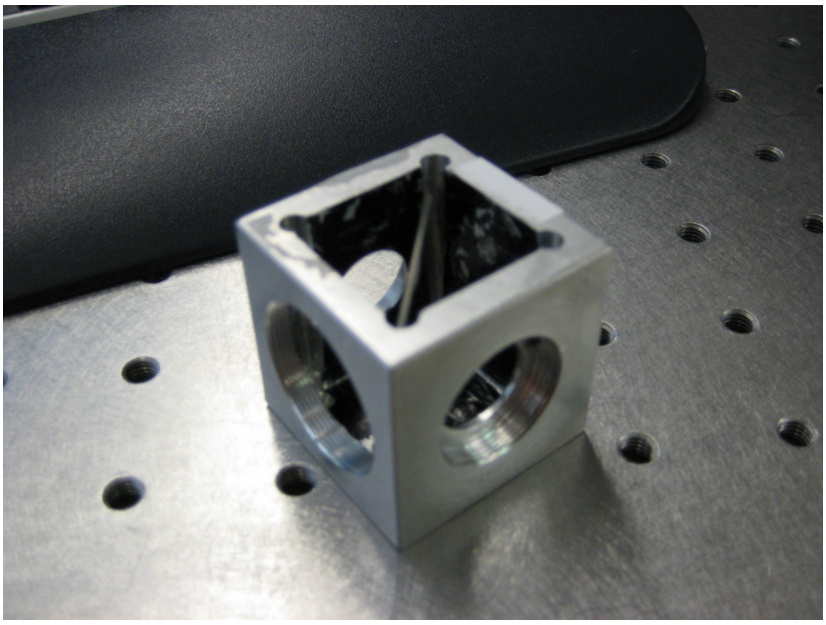

Figure 4.3: The "Cube" with beam splitter placed inside

This is a cube shaped component in the centre of "T" as shown in figure 4.3. It is designed to hold a specially designed rectangular shaped beam splitter which can be slid into the cube from the front face (as in figure 4.1), at an angle of 45°. It is made hollow, tapped and drilled in circular fashion on 3 side faces (top, bottom and left) so that light beam can travel to and from the beam splitter. The face on the right acts as a power dump. The top and left face provide circular tapping for circular cylinder shaped assemblies described next. The bottom face provides tapping for a microscope objective meant to focus and gather light to and from the sample. The front face is tapped square while the one at back is left untapped. The front face has little crevices inside its edges such that it can hold the beam splitter.

b) Input/ Output Tubes

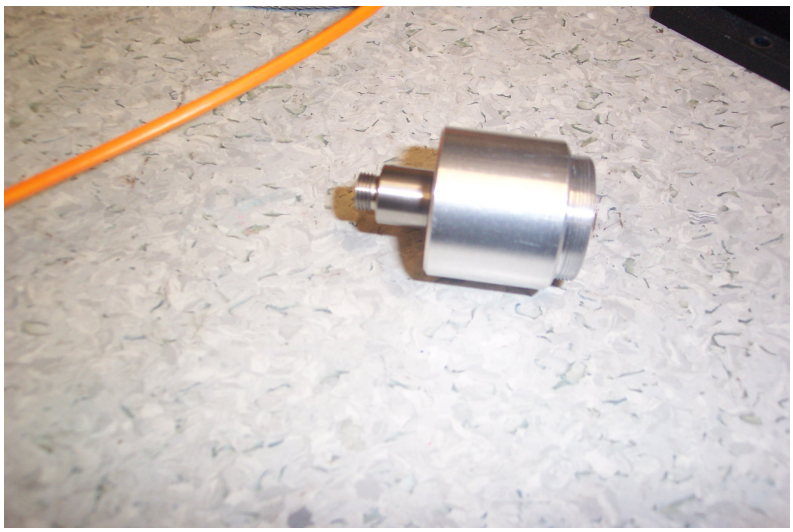

Figure 4.4: Cylindrical tube with collimator at left-most end and filter inside

These are circular cylinder shaped assemblies as shown in figure 4.4. These act as the input and output ports for the light coming/going through the optical fibers as shown in figure 4.2. One on the left is input from the laser source while one on top is output going to the detection system.

Their purpose is to hold in them optical filters, suitable for the input and output sides. They also provide tapping for optical collimators. Both the cylinders are designed in similar fashion. They are first drilled right through. One end provides tapping for the optical collimator. A slightly larger cavity is created on the inside of the cylinders to accommodate the optical filters which are in the shape of rings. After placing the filters in their respective cavities, the cavities are sealed to hold the filters in place to prevent them from falling over or getting tilted. This is done by screwing in specially designed metal rings. The cylinders are then screwed onto the faces of the cube. Important consideration is made to determine the distances between optical components.

4.2.2 The optical components used

All the optical components integrated in the "T" are described here and marked by arrows in figure 4.1.

- **Filters**

a) "Laser line"

This filter is integrated in **"input tube"** and placed next to the optical collimator. Collimated light coming from the collimator meets this filter next. The purpose of this filter is to provide a narrow band around 532nm radiation and to stop all other wavelength in their path.

b) "Raman edge"

It is placed in cavity of **"output tube".** This particular filter provides a stop-band just before the wavelength of incident radiation i.e. 532nm and has a broad-band that allows to pass through radiations above 532nm consisting of 'stokes' scattered photons. Scattered light consisting of 'Raman' and 'Rayleigh' photons before meeting the output collimator meets this filter which rejects the 'Rayleigh' component and lets pass 'Raman' through it.

- **Beam splitter (Raman reflector)**

It is a specially designed rectangular plate of glass. It is placed in the cube making 45° with its edges. On one of its two sides, a tiny reflecting circular mirror is etched in the middle. The dimension of this mirror is comparable to the beam-width of laser light.

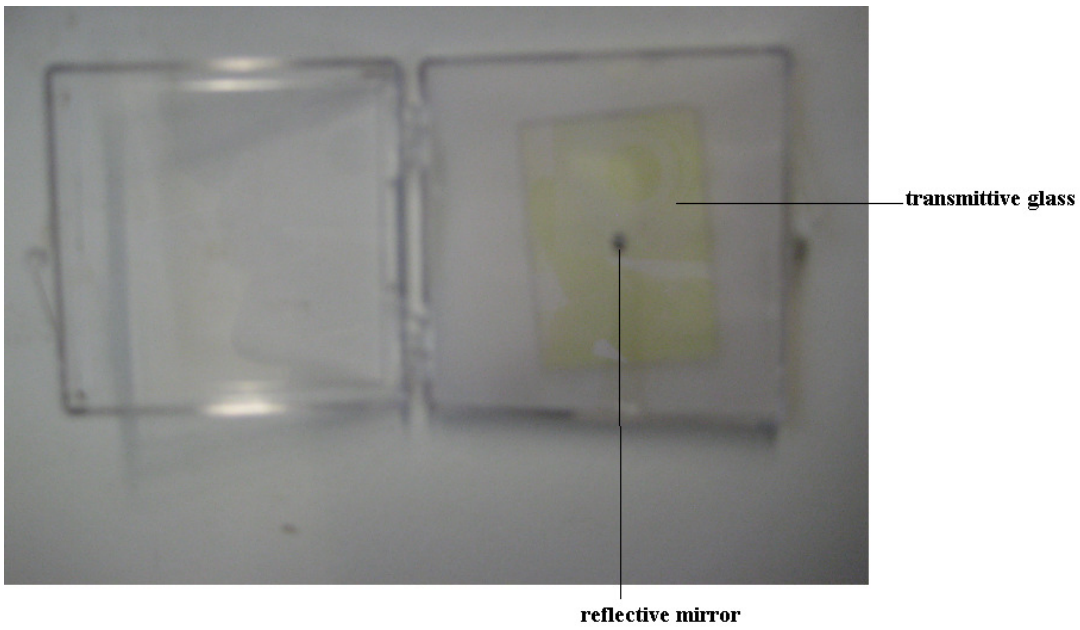

Figure 4.5: Beam splitter in its casing with tiny mirror in centre

The beam splitter carries out two important functions. Firstly, the tiny mirror **reflects** the incident laser light such that both incident and reflected beam makes an angle of 45° with the normal. Thus the reflected beam is sent in a direction perpendicular to the incident beam and is traveling in the direction of the sample. Secondly, beam splitter **transmits** the light scattered by the sample to pass through it and reach the optics at the output port.

- **Optical collimator**

The optical collimator on the input side is connected to the fiber bringing in the laser light. Thus it collimates the incoming light beam before it begins to disperse.

Similarly, on the output side it collimates the light beam coming from the output tube so that it could send with minimum loss in the fiber attached to the detection system.

- **Microscope Objective**

It is a system of lens which provides magnification of the object being observed. It has been made use in our Raman system in a novel way. Light coming from the beam splitter is though narrow but it is often needed to be further focused on a miniscule portion of the sample. To do this, the sample is kept at the focal point of the objective which allows the light beam to be focused on the sample.

Secondly, the raman scattered photons of light are emitted from the sample over a wide angle. The high numerical aperture objective gathers these photons and collimates them into a large diameter beam and sends it forth.

4.2.3 Laser source

Several types of lasers can be used as the excitation source for Raman spectroscopy. They are Ar+ ion (488.0 and 514.5 nm), Kr+ ion (530.9 and 647.1 nm), He:Ne (632.8 nm), Nd:YAG (1064 nm), and diode (532, 630 and 980 nm) lasers. Due to recent advancements in diode laser technology, it is the best candidate to be utilized in low-cost, portable Raman analyzer systems because of its relatively low cost, compact size and high reliability (>10,000-h lifetime) (Lam, 2004).

The laser used by us is a frequency doubled Nd:YAG laser. It has a visible wavelength of 532nm and 40mW of output power

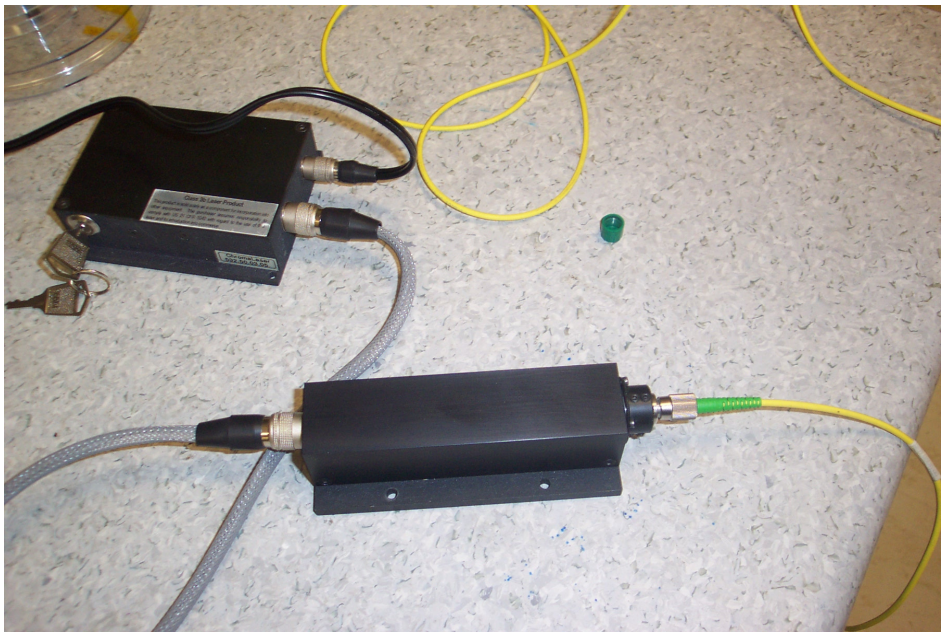

Figure 4.6: The used 532nm laser source

4.2.4 Optical fiber

The fiber cable used for the spectrometer is a special SMA-905 terminated optical fiber from Ocean Optics Inc. It's a 300µm core-diameter fiber. The buffer material used is polyimide with a cladding thickness of 15 µm. It has high OH content and is most efficient in 300-800nm (UV-VIS) range.

The laser source uses a single mode fiber with an FC connector.

4.2.5 Spectrometer

An Ocean Optics spectrometer called USB2000 with a fiber-optic input is used. It has been described in detail in section 3.2.2. It is an integral part of the detection system.

4.2.6 The 'Spectra Suite' software from Ocean Optics

The Ocean Optics spectrometer software called 'Spectra Suite' provides spectrum as a function of wavelength. It has been described in detail in section 3.2.2.

4.3 Operation of the system

Having looked at the system components in detail in section 4.2, the working of the Raman system is discussed here. Figure 4.6 shows the actual Raman system developed.

A single mode optical fiber is fitted to the outer end of the fiber collimator on the **input tube**. It transmits the monochromatic light beam emanating from the laser source into the collimator first. The optical collimator collimates the light beam and sends it forth to the laser line filter placed inside the cavity of the cylinder. The light beam meets the 'laser line' filter before it could disperse. The beam is narrowed down in the vicinity of 532nm and passes through the filter. Any laser noise and resonances are also prevented by the filter to pass through it.

The filtered monochromatic light beam now enters the cube. The height and angle of the beam splitter is carefully adjusted so that the beam could accurately impinge the tiny reflecting mirror etched in the middle of beam splitter. Since the beam splitter is placed at 45° to incident light, light beam is reflected at 90° and is sent into the microscope objective. It travels down through the objective and is focused onto the sample placed at its focal point. The sample position can be easily adjusted as it placed on the bench top. At this point, the incoming light has traveled its distance.

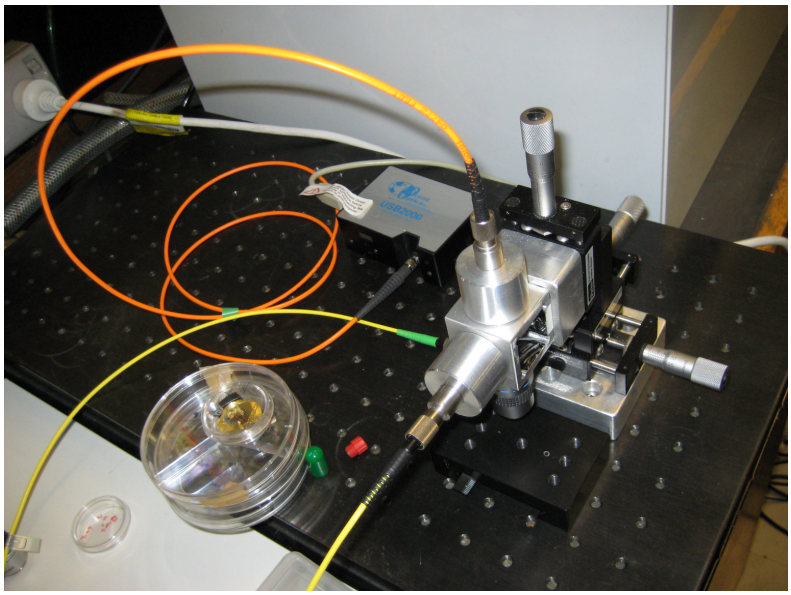

Figure 4.7: The custom built Raman spectroscopy system

Light interacts with the illuminated area on the sample and causes excitations in the system. This results in scattering of light in all directions over a wide angle. The scattered photons possess energy at, above and below the energy levels of the exciting light in accordance with the transition of electrons to different levels. Some of the scattered light reaches the objective lens which converts it into a parallel beam possessing larger beamwidth than the exciting laser beam. This beam travels further into the objective and reaches the centre of the beam splitter. Barring a smaller fraction which is obstructed by the reflecting mirror (approx. 10%), most of the light is transmitted straight through the transparent beam splitter. The transmitted light travels further into the output cube. It first encounters the "raman edge" filter, whose job is to filter Raman (energy different to exciting photons) scattered photons from Rayleigh (energy same as exciting photons) scattered photons. It does so by providing a sharp pass-band right on the edge of the laser line at 532nm. In this way, it allows all the photons having energy less than the Rayleigh scattered photons and filters out all other photons. As a result, the light is left to be composed of **stokes** Raman lines. This light reaches the fiber collimator which collimates it and passes it into the output fiber. The output fiber is in turn connected to the spectrometer. This light is detected by a CCD detector in the spectrometer. The photon count is converted to a digital signal as a function of wavenumber and can be observed on the software screen.

4.4 Important features of the developed Raman system

a) Sample mounting

Instead of mounting the sample on a traditional x-y-z three axis translational stage, the entire metal T assembly was mounted on a three axis translational stage with microscope objective facing down as in figure 4.2. The sample is placed under the objective on the bench-top. This not only allows precise control of region of the sample to be analyzed, but also has the advantage of keeping handling of delicate samples to minimum.

b) 'No moving parts' Raman system

An essential feature of the built Raman system is that it consists of effectively no moving parts. All the optical components required for a Raman system to function are enclosed in one assembly. This keeps them safe from any external damage. The sample only needs to be moved in proper position.

These components singularly need to be aligned at specific angles, heights, distances. The T-shaped assembly is designed such that it combines the optical components in perfect order. Some of the specific considerations that have been taken are:

i) Fiber collimator is placed at a distance suitable to collimate the light coming from the optical fiber connected to the laser source. It does so before light begins to disperse.

ii) Next, the laser line filter needs to be perfectly perpendicular to the direction of the light. This has also been taken care of.

iii) The beam-splitter has to be perfectly stationed at 45 degrees angle to the incoming light.

iv) More so, the light beam needs to impinge on the reflecting mirror which is just about the diameter of the light beam. This calls for the precise control over the positioning of the beam-splitter. Once these and similar settings have been taken care of, it could result in a Raman system which is unaffected by human interferences which can be an issue from time to time for the optical bench based systems.

c) CCD (charge-coupled device) based detection

The Ocean Optics spectrometer used for the Raman system consists of a CCD detector. Because the CCD detector multiplexes the Raman spectrum, the spectrum can be obtained in a shorter amount of time than is needed with a scanning monochromator. This is discussed in detail in literature review in section 2.2.5.

d) Portable and on-line systems

It is a useful guide to a technology coming of age when previously apparently complex instruments can be packaged in a suitcase suitable for air transport and

collected from the carousel. The suitcase is opened at the site of investigation and the system is put to work.

4.5 Establishing the developed system can actually do Raman spectroscopy

To establish how good a raman system the one developed is, a set of experiments have been done on samples such as that of paracetamol and polystyrene. These materials are known to produce Raman lines which not only have acceptably strong intensities but are also good in number. Thus it was thought that these samples could provide a good platform for experimentally testing our Raman system. Moreover, a comparison has been made of results from the developed system with the likes of other results obtained from reference. This is deemed useful in establishing the qualities and short comings of the developed system.

4.5.1 Some safety precautions needed when doing Raman spectroscopy

While doing the experimentation, some of the safety precautions taken are highlighted here.

a) The beam emanating at the sample end has enough energy to cause temporary or permanent damage to the eye. Appropriate laser safety goggles should be worn when lining up the apparatus and when inserting the samples in the beam.

b) One should never stare in the laser beam.

c) Care should also be taken when handling the sample. Gloves should be worn when handling sample, microscope objective, glassware or chemicals.

4.6 Experimentation on paracetamol

The first sample taken for the purpose of Raman investigation is an as-obtained tablet of paracetamol. In this section, the molecular structure of paracetamol is discussed. Raman spectroscopy of paracetamol is carried out and compared with suitable references. An attempt has been made to assign the obtained raman peaks to different bonds in the molecular structure of paracetamol.

4.6.1 Molecular structure of paracetamol

Since Raman is a fingerprinting technique, it is desirable to know the molecular structure of the substance being analyzed in order to successfully decipher the Raman spectrum obtained from it. The molecular structure is provided in figure 4.7.

It consists of a benzene ring core, bi-substituted by one hydroxyl group and the nitrogen atom of an amide group in the *para* (1, 4) pattern. The amide group is acetamide (ethanamide). It is an extensively conjugated system (a system of atoms covalently bonded with alternating single and double bonds (e.g., C=C-C=C-C)), as the lone pair on the hydroxyl oxygen, the benzene pi cloud, the nitrogen lone pair, the p-orbital on the carbonyl carbon and the lone pair on the carbonyl oxygen are all conjugated (Thorley, 2005).

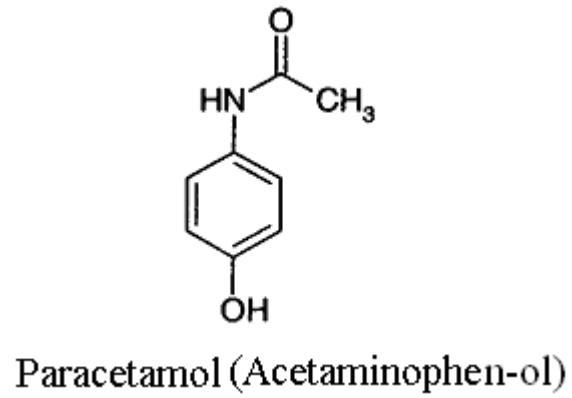

Figure 4.8: The molecular structure of paracetamol (Thorley, 2005)

4.6.2 Raman spectroscopy of paracetamol, from literature

Before proceeding to test the Raman system, it was thought desirable to know the results available in suitable literature. One such spectrum obtained by (Al-Zoubi, 2002) is shown in figure 4.8. The spectrum shows several raman peaks. Prominent peaks have been numbered with their approximate raman shift wavenumbers.

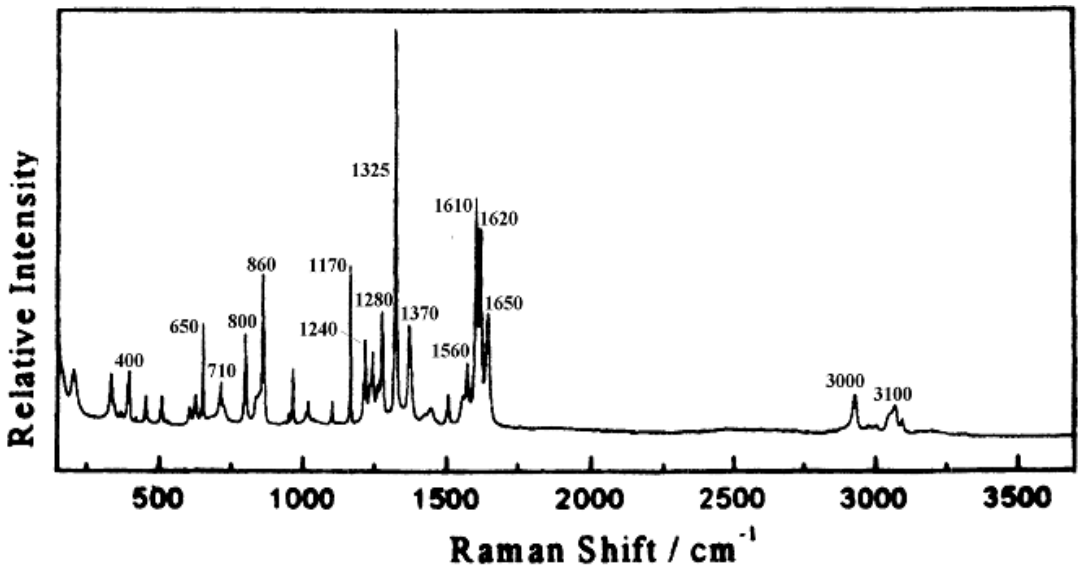

Figure 4.9: The Raman spectrum for paracetamol (Al-Zoubi, 2002)

4.6.3 Experimentation: Raman results from paracetamol

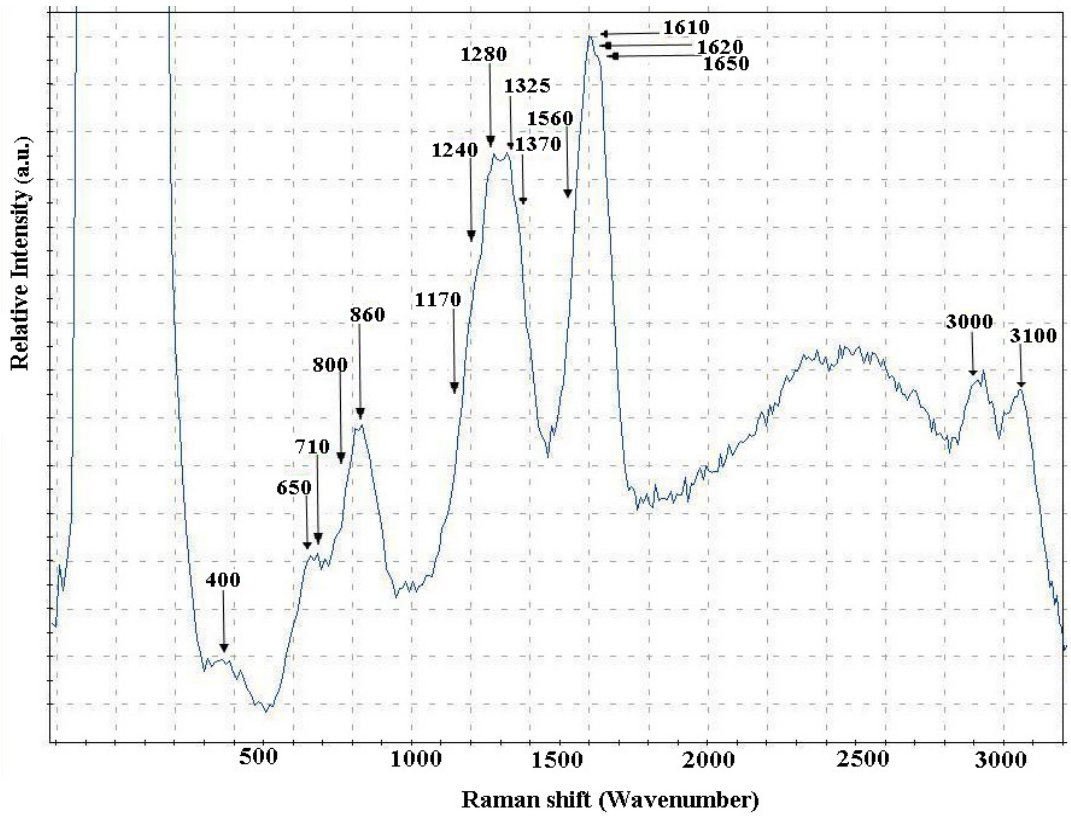

Figure 4.10: Raman spectrum obtained for an as-obtained tablet of paracetamol

Having known the raman spectrum to be obtained from a literature source, the build raman spectroscopy setup was put to test to observe its performance and compare it against that obtained from literature.

For this purpose, an as-obtained tablet of paracetamol was used as the sample. It is worth mentioning at this point that raman spectroscopy requires hardly any sample preparation (Pitt, 2005). The Raman results obtained for a tablet of paracetamol by the designed system is shown in figure 4.9. The acquisition time, because Raman scattering is very faint, is set for 5sec with averaging set for 10 exposures; a single measurement takes about 50sec.

.

4.6.4 Discussion of the Raman results

Figure 4.9 shows the position of the stokes bands which are characteristic of the photons possessing frequency lower (or higher wavelength) to the frequency of the photons elastically scattered (rayleigh lines). Comparing the raman spectrum obtained here with the one taken from reference in figure 4.8, a few observations can be made which highlight some similarities and a few dis-similarities. These observations are discussed.

4.6.4.1 Observation of broad bands instead of fine lines

The lines in the reference spectrum are finer in width covering only a few (1-10cm^{-1}) wavenumbers and also are well separated (i.e. well resolved) while in the experimental result of figure 4.9 these appear to combine together to give quite broad bands covering a few 10's to upto 100 wavenumbers.

The poor resolving power of the detector (approx 80cm^{-1}) available at hand is the most valid reason that could be given for the poor resolution of Raman lines. The USB2000 spectrometer was discussed in detail in section 3.2.2. The large value of resolution of the spectrometer could be confirmed from an observation of a few lines in figure 4.9. For example: 710cm^{-1} is 90cm^{-1} apart from 800cm^{-1} peak and thus are well resolved from one another. Again, 3000cm^{-1} is resolved to 3100cm^{-1} by 100cm^{-1}. On the contrary, 650cm^{-1} is not well resolved from 710cm^{-1}, the difference being only 60cm^{-1}

in this case. Again, 1610cm^{-1} is not well resolved from 1650cm^{-1} due to similar reasons.

With the current specification for the spectrometer, it is known to have good sensitivity but poor resolving power which puts a question mark on use of this spectrometer for raman measurement purposes. Given that it is one of the cheapest available spectrometers around possessing acceptable features, its use in a low cost application for doing basic raman spectroscopy is pretty significant. There are higher models of spectrometers available but their cost is much higher. This would defeat the sole purpose of building a cost-efficient raman spectroscopy system.

4.6.4.2 The observed raman bands assignment

Despite poor resolving power of the spectrometer at hand, quite a few raman peaks are well observable which justifies the use of this spectrometer. Comparing the figures 4.8 and 4.9, these raman peaks are found to match fairly closely.

Appearance of each of the raman peaks in figure 4.9 is representative of one or the other chemical bond in the molecular structure of the sample. Different chemical bonds undergo different changes in polarizability (vibrational or rotational distortion such as bending or stretching) as they receive energy from the exciting source. The mechanism of Raman excitations is discussed in detail in section 2.2.

Making use of suitable references (Grasselli, 1980; Lin-Vien, 1991; Kachrimanis, 2007 and Moynihan, 2002), attempt has been made to assign the observed raman bands to different bindings in the molecular structure of paracetamol. Assignment has been done for many of the bands barring a few which could not be assigned with certainty.

Table 4.1: Bands observed and their assignment to molecular bonds

Bands observed (cm^{-1})	**Band assignment to functional group**

400	**400 :** Not distinguishable
600-700	**650, 710:** Not distinguishable
800	**800, 860:** Not distinguishable
1100-1400	**1170, 1240, 1280:** associated with aromatic (–C-N) and (–C-O) stretching vibrations. **1325:** C-N symmetric stretch **1370:** symmetric bend (CH_3)
1550- 1650	**1560:** amide (N-H in-plane deformation) **1610,1620, 1650:** skeletal aryl C=C stretch, skeletal aryl C-C stretch and amide carbonyl respectively
3000-3100	**3000:** (-C-H stretch) **3100:** stretching of N-H bond

4.6.4.3 Distinguishing 'relative' intensity count to absolute intensity count in a raman spectrum

Referring to figure 4.8, it can be seen that y-axis doesn't give any specific intensity numbers in terms of photon counts but simply states intensity as 'relative intensity' or 'intensity (arbitrary units)'. Review of other papers (McCreery, 2002 and Day, 2003) providing raman results suggest different values for intensity or intensity in arbitrary units or simply no units at all. However, different authors seem to agree on 'relative intensity' of these lines to each other.

This supports the fact that it is not always necessary and advisable to obtain a specific intensity count for these lines because different experimenters use different set of parameters such as integration time (time to accrue photons at the detector) to obtain the raman signal. This implies that identifying these lines according to their relative intensities is sufficient for the purpose of assignment of lines to functional groups that make up the chemical composition and cause these lines to appear.

4.6.5 Conclusion

It was establish that the raman system developed was able to provide raman spectrum for a sample of paracetamol, although the obtained spectrum was found to be lacking in details regarding the acquirement of individual lines. This drawback is most certainly due to the poor resolving power of the spectrometer available at hand. Using a spectrometer with greater optical resolution and better sensitivity will result in far detailed raman spectrum but this would sky-rocket the cost of the whole system and would defeat our very purpose of developing a low cost raman system.

4.7 Experimentation on polystyrene

Another sample tested by the custom built raman system is polystyrene. The molecular structure is discussed first and then raman spectrum for polystyrene is ascertained through a reference. Raman spectroscopy result is provided and discussed with the help of reference.

4.7.1 The molecular structure of polystyrene

Polystyrene is an aromatic polymer made from the aromatic monomer styrene. Styrene, also known as vinyl benzene, is an organic compound with the chemical formula $C_6H_5CH{=}CH_2$. Polystyrene sample is available in the form of plastic petridish in most chemical processing labs.

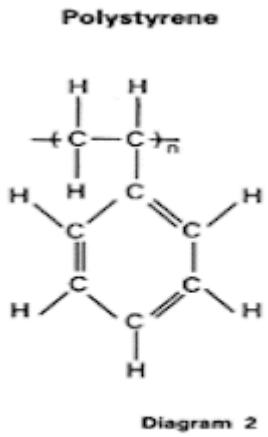

Figure 4.11: Molecular structure of polystyrene (Lam, 2004)

4.7.2 Raman spectroscopy of polystyrene, from literature

Similar to paracetamol, polystyrene is another substance which is easily available and can be used to establish the working of the raman system. The figure 4.11 is a raman spectrum obtained from polystyrene taken by a reference author (Lam, 2004).

Raman spectroscopy of polystyrene was carried out to validate the result from figure 4.11 and to confirm the operation of the designed system. Comparing the result obtained in figure 4.12 from polystyrene to that from figure 4.11, the peaks shown by our measurement are found to match very closely with those observed in the reference.

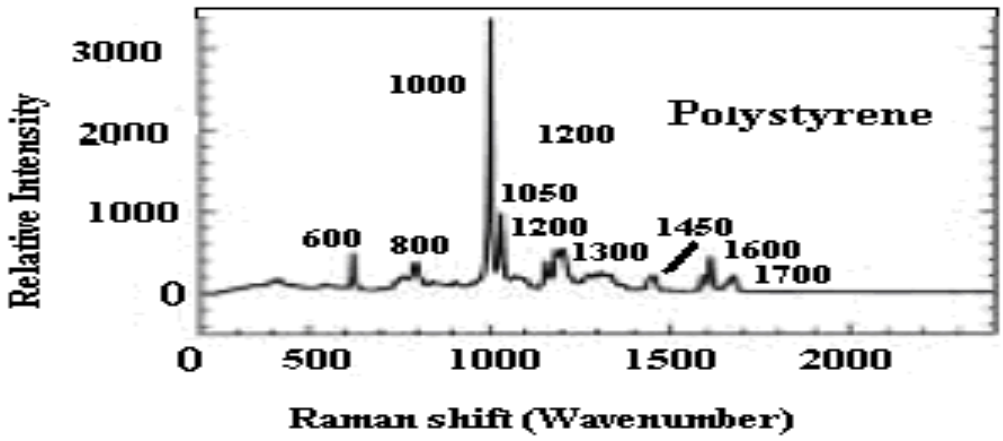

Figure 4.12: Raman spectrum of polystyrene (Lam, 2004)

4.7.3 Experimentation: Raman results from polystyrene

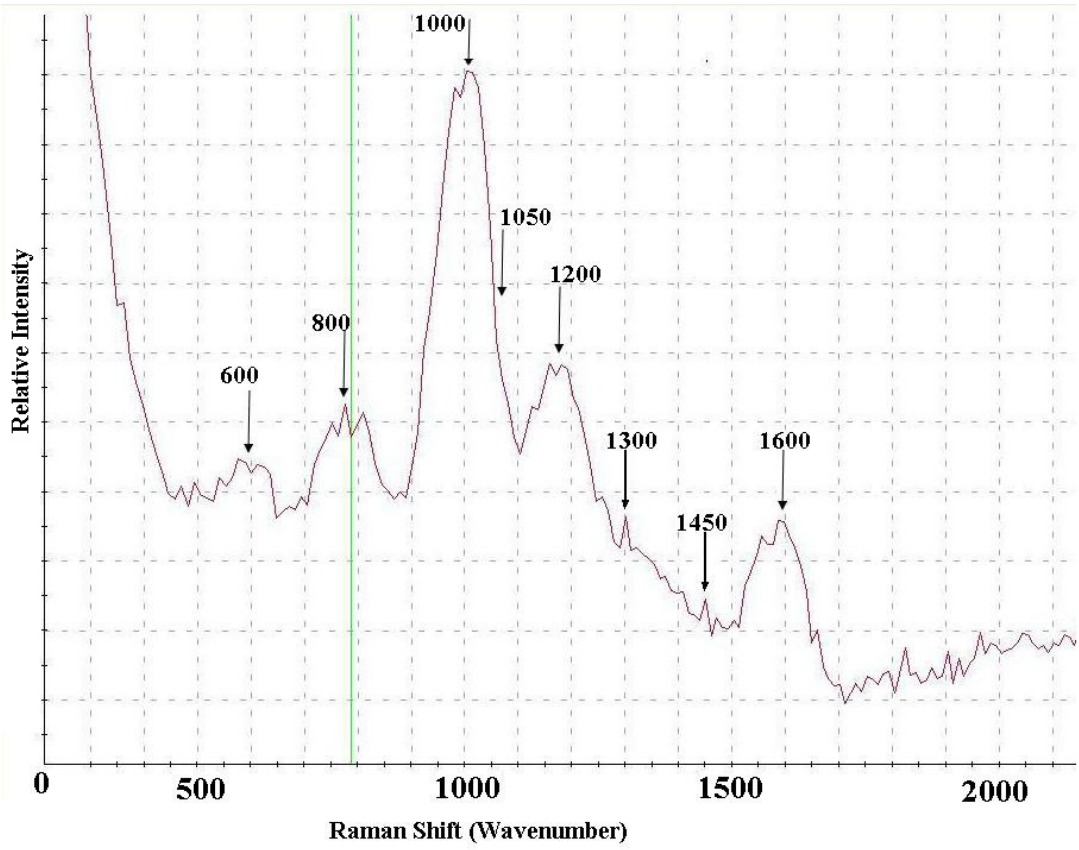

Figure 4.13: Raman spectrum obtained for a sample of polystyrene

4.7.4 Discussion of the results

Almost all the raman lines shown by the experimental spectrum in figure 4.12 are found to match closely with those from reference given in figure 4.11.

The resolving power of the spectrometer is further confirmed here to be in the region of 80cm^{-1}. To confirm this point, examples of peaks in figure 4.12 can be taken. Peak at 1000cm^{-1} is not well resolved from 1050cm^{-1} but 1200cm^{-1} and 1300cm^{-1} can be distinguished pretty well.

4.7.4.1 Assignment of raman bands of polystyrene to functional groups

Similar to paracetamol, an attempt has been made here to assign the observed raman bands to bonds comprising the molecular structure of polystyrene with the help of references as (Grasselli, 1980 and Lin-Vien, 1991). These bonds undergo vibrational changes as they receive energy from the exciting source.

Table 4.2: Band peak location and assignment to functional group

Band peak(cm^{-1})	**Band assignment to functional group**
600	monosubstituted benzene ring deformation.
800	stretching vibration of aliphatic chain of (-CH-CH_2-).
1000	(-C-C) stretching vibration of aromatic chain.
1050	in plane (-C-H) deformation.
1200	in plane (-C-H) deformation.
1300	(-CH_2) twisting vibration.
1450	(-CH_2) bending vibration.
1600	aromatic ring stretches (doublet).

4.7.5 Conclusion

From the results obtained for polystyrene coupled with the result from Paracetamol, it can be confirmed that a raman system that is not just capable of providing acceptable results but also is cost effective has been developed. However, it can be developed further as and when the need arises.

4.8 A drawback of raman spectroscopy: Fluorescence

This section describes fluorescence which can be a major drawback on certain occasions when carrying out raman spectroscopy. Also, some possible ways of its eradication/reduction are also discussed.

Fluorescence can be a major problem with the analysis of certain samples especially pharmaceutical compounds by raman spectroscopy. It is caused by either the dosage sample itself or a small amount of impurity present in the sample. Fluorescence is basically a luminescence due to the molecular absorption of a photon triggering the emission of another photon with a longer wavelength. The fluorescence emission of aromatic molecules, either the drug substance or an associated impurity, generally occurs in the near-UV to visible (300nm–700nm) region and therefore can interfere with the Raman signal if it is located within that spectral region (Vaughan, 2004).

4.8.1 Ways to eradicate/reduce fluorescence

There are two ways of possibly reducing/eradicating fluorescence emission. These are:

a) Use of laser source in UV or Infra-red

Since the scattering depends on fourth power of frequency, the obvious way to improve Raman sensitivity is to use highest frequency laser lying in UV region. UV has the advantage of causing less fluorescence than visible but at the same time, many compounds absorb UV radiation (Smith, 2005) which can be a hurdle when using this technique.

Also high energy photons increase the risk of sample degradation. Near IR laser is also known to reduce fluorescence but its use puts a limitation on the range of CCD detectors (Robinson, 2004).

b) SSRS ("Scissors")

(Bell, 1998 and 2000) provides evidence of yet another means of getting rid of fluorescence. This technique called Subtracted Shifted Raman Spectroscopy (SSRS) is a mathematical iterative approach to obtain faint raman peaks by subtracting spectra obtained from two different positions of spectrometer.

c) Photo-bleaching

Photobleaching is a process of exposing the sample to intense laser power for some time duration (MacDonald, 2006). Photobleaching was carried out for a sample of Paracetamol. Figure 4.13 shows a typical set of spectra obtained from paracetamol sample. The top spectrum is taken integrated over 2s and number of scans taken to be 10 while one at the bottom is also obtained at the same integration time of 2s done over 10 scans, but after having exposed the sample to fully powered laser light for duration of 1h and no offset was applied to the ordinate axis in this presentation..

The original spectrum (uppermost trace) exhibits considerable background fluorescence. The lower trace indicates that 1h photobleaching at 100% power reduced the rising background such that the peaks can be seen against a flatter background. Mathematical techniques have also been proposed to remove the fluorescent background; however, such techniques do not improve the signal to noise ratio and therefore only make larger peaks more easily visible against the background and do not render smaller peaks more easily discernable against the inherent noise in the system.

Conversely, taking a spectrum over 1h of photobleaching was shown to improve the signal to noise ratio (SNR) and also reduce the fluorescence background and, therefore, the small peaks were better visible (MacDonald, 2006). In figure 4.13, there are five regions of improvement distinguished to be affected by photobleaching. These are discussed as:

- **Local improvement in SNR of peaks**

Reduction in fluorescence led to improvement in the signal-noise ratio of peaks. After photobleaching, the intensity count was improved from 375 intensity counts to approximately 500 intensity counts for one of the peaks in figure 4.13.

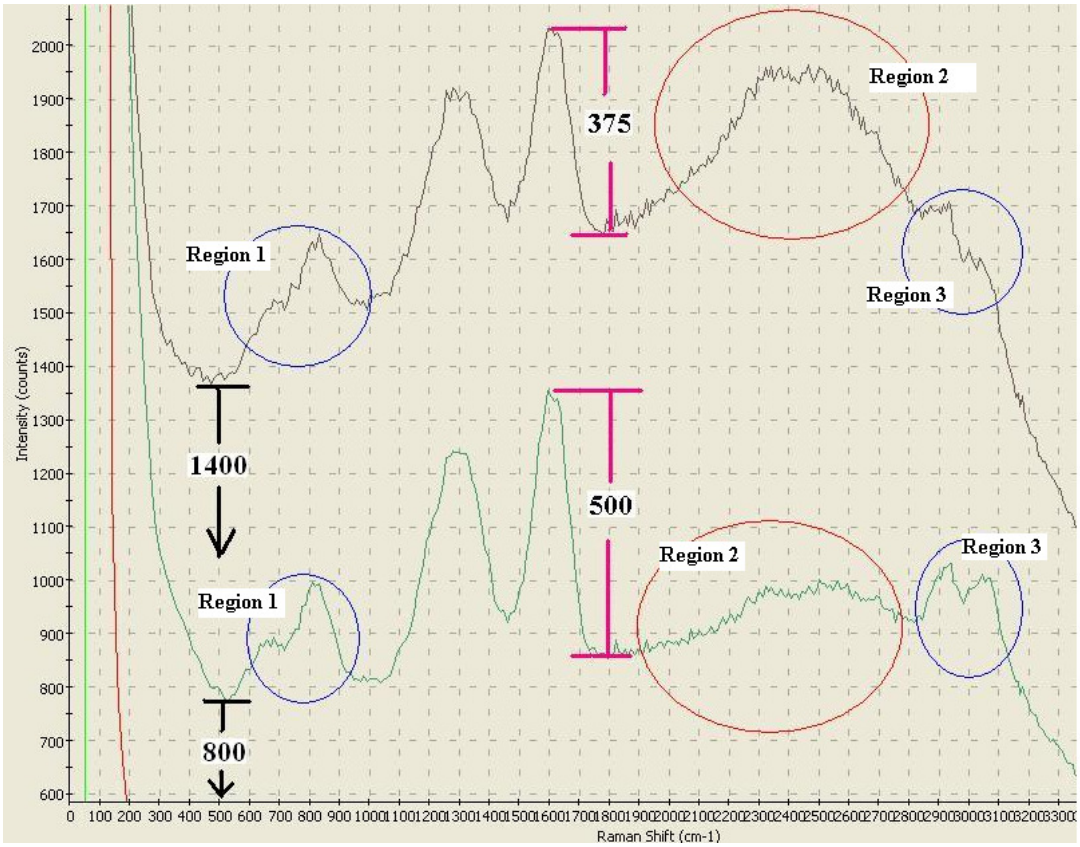

Figure 4.14: The 'spectra-suite' window depicting photo-bleaching process

- **Improvement in SNR of the entire spectrum**

Photobleaching has not just reduced the local fluorescence effect for individual peaks but also improved SNR over the entire range of wavelength. This has led to reduction in elevation of the spectrum from approximately 1400 intensity counts to 800 intensity counts, over the baseline of '0' intensity count.

- **Regions 1 & 2**

Raman peaks which were not well resolved under the influence of fluorescence appear to be better resolved after photobleaching. There is a marked improvement in the SNR of these peaks as well.

- **Region 3**

This region is a direct consequence of doing photobleaching. Paracetamol is not known to show raman lines in region 3. This means that the wide band observable in top spectrum must be due to fluorescence. In bottom spectrum, this band was observed to reduce considerably.

It was observed that exposure for another hour reduced the fluorescence further. This reduction, however, was much less compared to the reduction achieved in the first hour. It can be concluded that prolonged exposure to laser energy would help reduce fluorescence further but the process would follow a decreasing exponential rather than a linear relationship as was also discussed in a few references (MacDonald, 2006 and Vaughan, 2004).

It should be noted here that the reason for obtaining lower overall intensity count in figure 4.13 compared to figure 4.9 is that these spectra were obtained at a reduced integration time of 2s unlike earlier case which was carried out for 5s integration time.

4.8.2 Conclusion

In this section, fluorescence which could be a major hurdle in some raman measurements and possible ways of reducing it are discussed. Photobleaching as an effective technique of fluorescence reduction is implemented and discussed. Fluorescence is found to reduce after having done photobleaching at full power for one hour. Regions in the spectrum which were influenced by photoleaching were identified.

Chapter 5: Plasmon Resonance and SERS

5.1 Introduction

Nano-structures of noble metals, such as Ag or Au, are known for their strong interactions with visible light causing resonant excitations of the collective oscillations of the conduction electrons within the particles. This mechanism is called plasmon resonance effect (Sherry, 2005 and Klar, 1998). In this chapter, fabrication of such nano-arrays of noble metals is discussed and plasmon resonance frequency is obtained using UV-Visible spectroscopic technique discussed in chapter 3.

Certain nanometer-scale architectures found in biological systems are known to produce a number of striking optical effects. It has been proposed to use these natural nano-structures as a basic tool for the fabrication of the metal nano-arrays.

Further in the chapter, we discuss **Surface Enhanced Raman Spectroscopy**, or **Surface Enhanced Raman Scattering**, often abbreviated **SERS**, as a surface sensitive technique that results in the enhancement of Raman scattering by molecules adsorbed on rough metal surfaces. The enhancement factor can be as much as 10^{14}-10^{15}, which allows the technique to be sensitive enough to detect single molecules. The exact mechanism of the enhancement effect of SERS is still a matter of debate (Liang, 1997) in the literature but here an attempt has been made to achieve and explain SERS by adsorbing certain adsorbate on the Ag nanostructures arrays.

Although Surface Plasmon Resonance has been widely studied since 70s and 80s of the last century, its use for the development of nano-optical sensors and near-field optics makes it a hot topic of research lately and the literature is building very rapidly (Pissuvan, 2006, Roy, 2004 and Hutter, 2004). A few research questions are asked in this chapter and attempt has been made to answer them in the best possible way through experimentation and with the help of available literature.

5.2 Certain biological systems possess nanoscopic structures

Wings of certain biological species such as cicada has been shown in (Watson, 2002 and Zhang, 2006), to possess nanoscale structures. The hypothesis is investigated here and results are provided.

5.2.1 Methodology

To investigate this research question, a few mm by mm sized segment of cicada wing was carefully cut from cicada wing. The cicada wings were cleaned to remove the stains. The cleaning procedure consists of two steps, whereby the wings were sonicated in acetone for 15mins to remove any organic compounds and dirt, followed by sonication for 20mins in de-ionized water. The wing segment was left to dry. After drying, the cicada wing was observed under a Scanning Electron Microscope (SEM).

Figure 5.1: A beautiful insect called 'Cicada (*Cicadetta celis)*'(Zhang, 2006)

5.2.2 Results and Discussion

The SEM images of cicada wings are given in Figure 5.2 and 5.3. The images confirm the presence of inherent nanostructures on the wings of cicada. These nanostructures appear to be in the form of vertical pillars having heights of ~400nm and diameter at the top ~100nm with interstitial gap ~150nm in between the structures. The

images provide other details such as accelerating voltage for the electron beam, spot size magnification and scale.

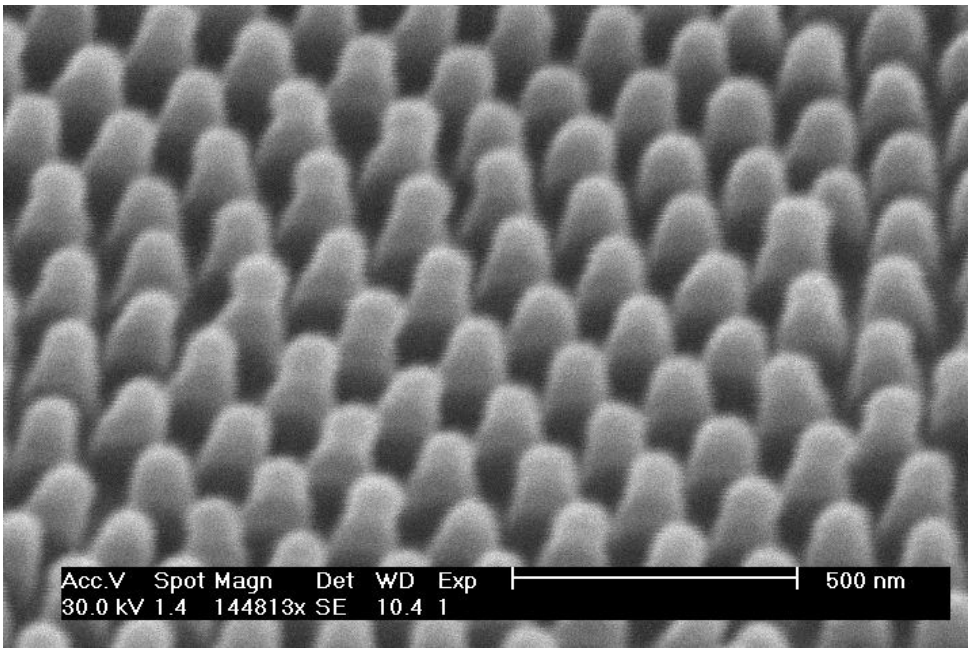

Figure 5.2: The SEM image showing side view of cicada wing

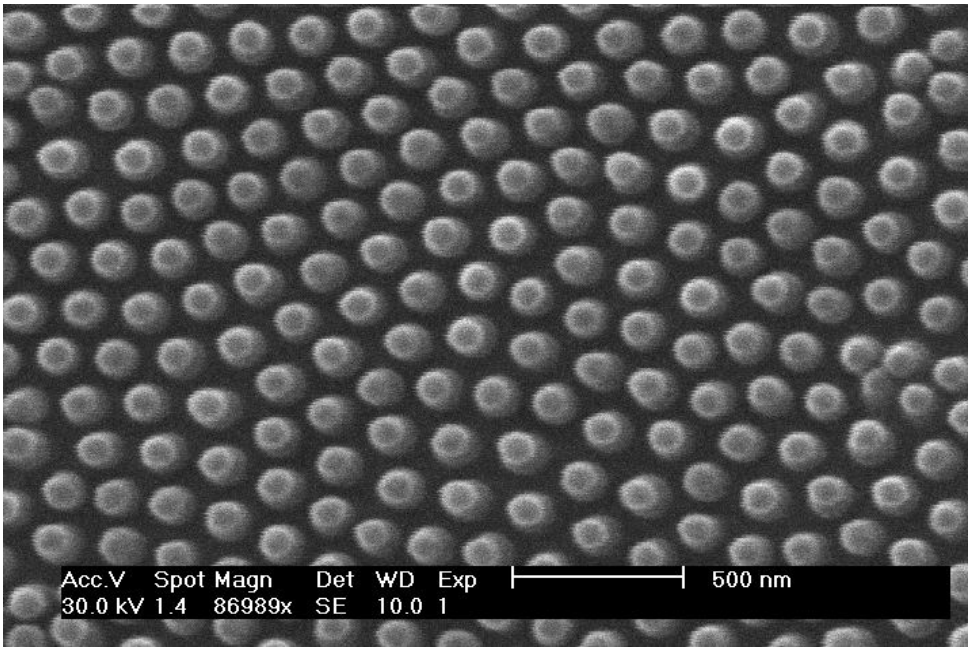

Figure 5.3: The SEM image showing top view of cicada wing

5.3 Fabricating metallic nanoparticles (eg. Au) on cicada wing

Having confirmed the presence of nanoscopic structures in section 5.2 on the wing of 'cicada', the next question to be asked is whether there is a possibility to use these nanoscopic structures as a template to deposit a metal nanostructure array. To investigate this hypothesis, the following methodology was adopted.

5.3.1 Methodology

A tiny segment of cicada wing was deposited with a layer of Gold (Au) using the electron beam evaporation technique. The thickness of the layer was taken to be approximately 200nm. The deposition was done close to normal incidence, at a slightly oblique angle of 30°. This was done to obtain metal particles which were well separated from each other. There was another deposition carried out at thickness of layer approximately 400nm. Yet another set of 200nm Au film samples were prepared at an oblique angle of 70°.

5.3.2 Result and discussion of Au film deposition

The SEM image of the 200nm Au film deposited wing was taken to investigate if deposition of gold film had resulted in formation of nanoparticles. The figure 5.6 shows the SEM image of cicada wing deposited with 200nm Au particles. Although the image looks blur, a careful observation would establish this deposition as an array of separate and continuous nano-particles, each nanoparticle being like spherically oblonged pillars deposited at an angle of 30°. Moreover, interstitial gaps can also be observed between most of these nanoparticles. Such a deposition resulted in a metal-dielectric(air)-metal-dielectric kind of a configuration. Later, it would be demonstrated that this type of configuration is necessary for plasmon resonance effect to take place.

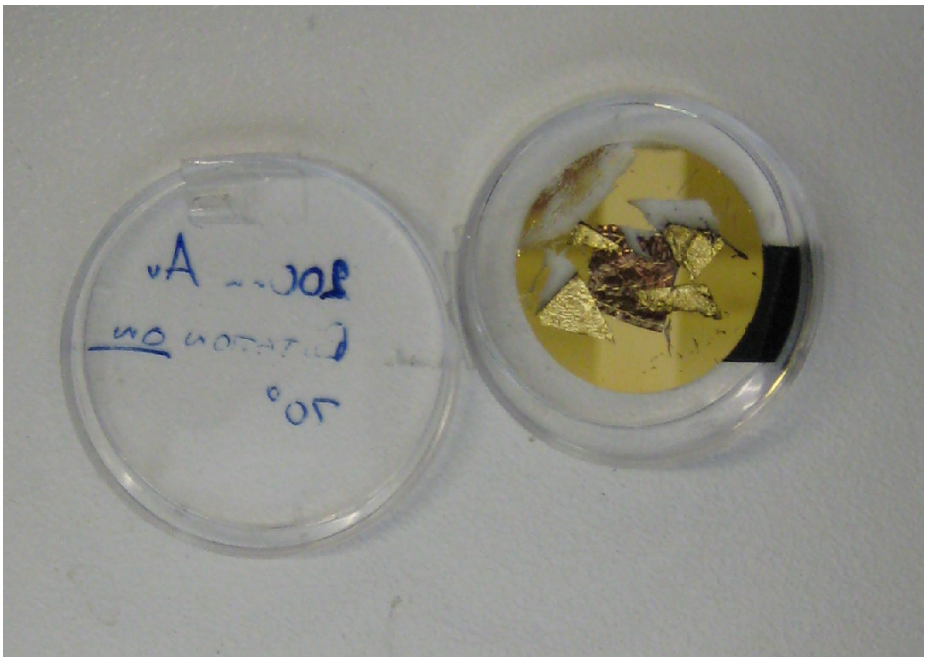

Figure 5.5: Cicada wing deposited with Au film

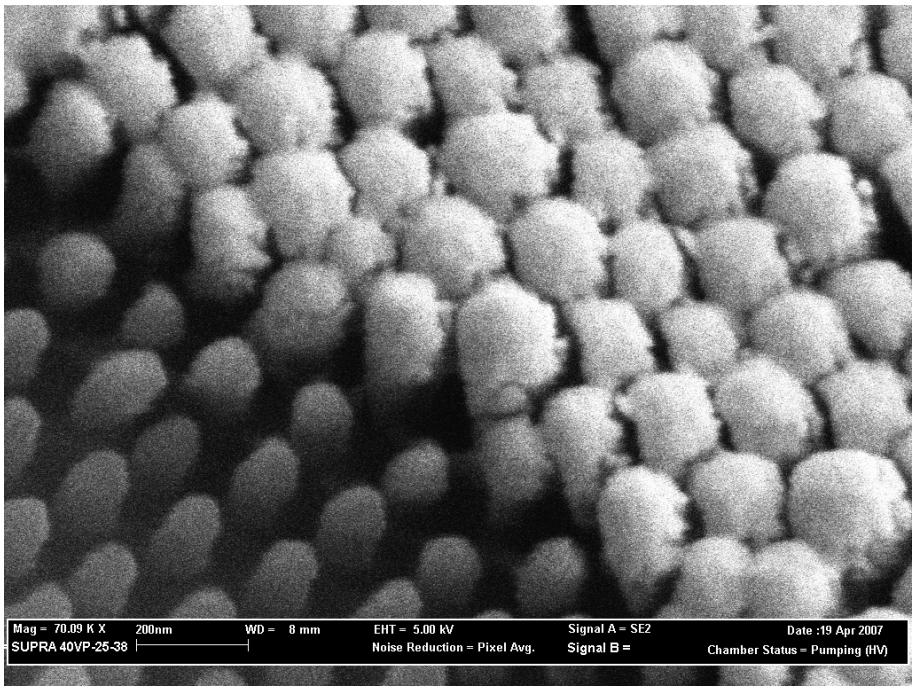

Figure 5.6: The (SEM) side view of 200nm gold layer on the cicada wing

5.4 Optical spectroscopy characterization

Having successfully deposited Au nanostructures onto cicada wing, the next task is to carry out spectroscopic investigations on deposited cicada wings. Experiments were carried out to observe plasmon resonance effect and other similar effects.

For the purpose of observing plasmon resonance effect for the Au nano-particle arrangement deposited on cicada wing, it was required to expose the arrangement to energy from some exciting light source. For this purpose, an optical characterization setup was configured. It was learnt from literature (Berciaud, 2005 and Mulvaney, 1996) that UV-Visible absorption spectrum was needed to describe the plasmon resonance effect for gold particles. The spectrum was obtained using an USB2000 spectrometer attached to an inverted microscope. The setup is same and follows the same methodology as described in section 3.2.1.3.

5.5 Experiment 1: Absorbance spectroscopy comparison of smooth Au film to Au nano-particles

In order to appreciate the plasmon resonance feature obtained for a 3-D array of gold nanoparticles, a sample of cicada wing was deposited with 200nm film of gold on it as has been discussed in section 5.3. It was decided to compare it with spectrum for a gold film deposited onto a smooth surface without any nanostructure on it. For this purpose, a 200nm gold film was deposited on a smooth glass substrate.

Absorbance spectroscopy was carried out for the two samples in the range of 400nm to 800nm. The optical characterization was also carried out on a sample of cicada wing which was washed and dried but was yet to be deposited with any gold.

5.5.1 Results

Figure 5.7 shows a set of spectra obtained for the 'absorbance' of light by the three samples.

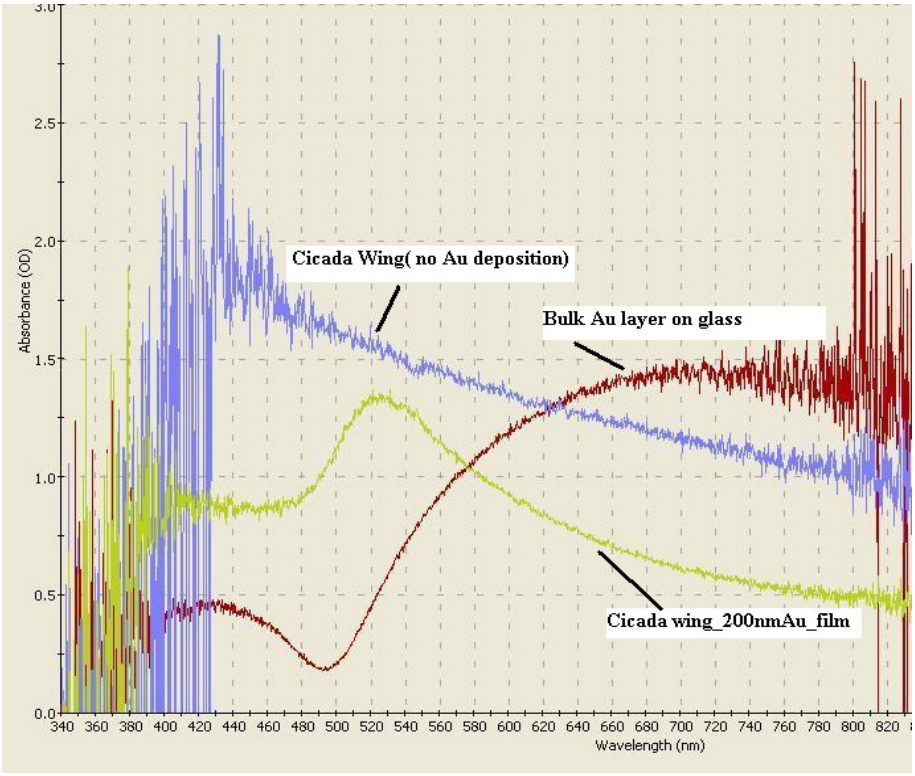

Figure 5.7: Spectra comparison for cicada wing, wing with 200nm gold film deposited and a smooth layer of gold deposited on glass substrate

5.5.2 Discussion: Understanding plasmon resonance mechanism

The light from the excitation source excites the particle plasmons. The excited collective electron oscillations within the particles then radiate electromagnetic waves of the same frequency into the far field, whereby the microscope objective is placed which does the collection. It sends the light forth to the output port of the microscope where the open end of fiber collects sends it to the spectrometer system and spectral measurement take place.

As said before, a 3D array of metal nanoparticles is deposited on the cicada wing structures. A cluster of metal nanoparticles placed in close proximity to one another and separated by small distances, form a metal-dielectric-metal-dielectric configuration, air being a dielectric medium in this case.

It is known from previous studies (Sherry, 2005 and Klar, 1998) that if such an arrangement of metal nanoparticles comes under the influence of electric field such as visible light, it strongly interacts through the resonant excitations of the collective oscillations of the conduction electrons within the particles. The excitation is quantized giving rise to quantized particles called plasmons. Such an interaction causes strong light scattering and enhancement of local electromagnetic fields causing the appearance of intense **surface plasmon bands** at plasma frequency. This mechanism happens because light of frequency below the plasma frequency is reflected since the electrons in the metal screen the electric field of the light. Light of frequency above the plasma frequency is transmitted, because the electrons cannot respond fast enough to screen it.

According to Kreibig (1985) et al., the optical properties of small particle samples are known to be mainly determined by two contributions:

(1) The properties of the particles acting as well-isolated individuals, and

(2) The collective properties of the whole ensemble.

Two types of interaction prevail between arrayed metallic nanoparticles: near field coupling (between particles that are close to each other) and far-field dipolar interactions The focus of our study revolves around the effects of near-field interparticle coupling on the particle plasmon resonances, especially the shift of the plasmon resonant wavelength as a function of particle size. Particles ranging from 200nm to 400nm size are investigated for this purpose.

5.6 Experiment 2: Plasmon peak position dependence on size of nanoparticles

The next set of experiment involved carrying out spectroscopy on two cicada wings with different size of Au nanoparticle film deposited on it. The two sizes taken here are 200nm and 400nm respectively. Figure 5.8 shows the spectra for the two sizes of Au nanoparticle deposited on cicada wings.

5.6.1 Results

Figure 5.8 suggests a red-shift in the absorption peak with increase in the size of gold particles. It can be seen that deposition at close to normal incidence (30°) resulted in an absorption peak centered at approx 530nm for a 200nm size particle and approx 550nm for a 400nm size particle, respectively.

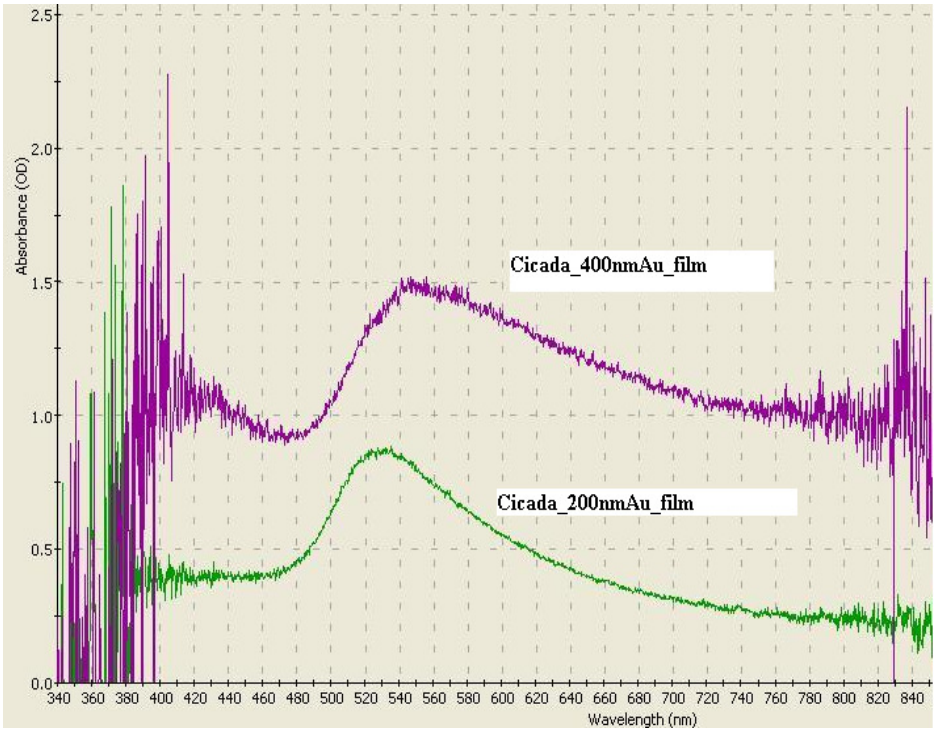

Figure 5.8: Plasmon resonance peaks for two particle sizes of Au on cicada wing

5.6.2 Discussion

Plasmon resonance mechanism and size dependency on absorbance peak's position is discussed in this section. Discussion is largely carried out with the help of available literature provided in the 'literature review' chapter.

This size increase of nanoparticles from 200nm to 400nm causes the distance between the nanoparticles to decrease when measured from the center of the particles.

It follows from Kreibig (1985) et al., that to determine the particle size effect on the plasmon peak positions, calculations are restricted to free-electron model. This

model states that a metal array of nanoparticles undergo various interactions and processes.

Kreibig (1985) et al., provides details of a number of material effects that work together and have been studied by various theoretical models. All/or some of these effects may combine to provide the overall shift in resonance band. These two tables are provided in appendix. These tables look confusing as there are predictions of shifts into both directions. However, there are some systematic features observed:

(i) Classical conductivity models predict **red-shifts** due to increased damping of the electron motion.

(ii) Volume plasma excitations cause **blue-shifts**.

(iii) Quantum size-effect theories including Landau damping also yield **blue-shifts**.

(iv) Regarding the electron density profile normal to the particle surface as smooth results in **red-shifts**.

The meanings of red and blue shifts should be noted at this point. Red shift means the shift of a wavelength to a higher wavelength i.e. moving closer to the red band of the white light. On the other hand, if a wavelength shifts to a lower wavelength i.e. closer to the blue band, it is termed as blue shift.

5.6.3 Conclusion

It can be concluded from the discussion that the red-shift we observe in figure 5.8 as the size of nanoparticles is increased, must be the overall effect arising out of the super positioning of various processes that take place in the array as it is excited by an illuminating light source.

These effects discussed in literature review on plasmon resonance effect and corresponding tables for various material effects and theoretical calculations for the same is provided in appendix.

5.7 Experiment 3: Effect of the angle of deposition

The cicada was deposited with Au film at two different angles this time. First deposition was close to normal (30°) to the sample surface and the other was at an oblique angle, 70°. Optical spectroscopy was undertaken and plasmon resonance bands were observed.

5.7.1 Results and discussion

There is not much evidence from the literature as to what happens to the absorbance peak position when the angle of deposition is varied. Comparing the spectra in figure 5.9 for two different angles of deposition, it is observed that the absorbance band has broadened but decreased in height (absorbance count), with the increase in deposition angle, while the overall intensity remains high.

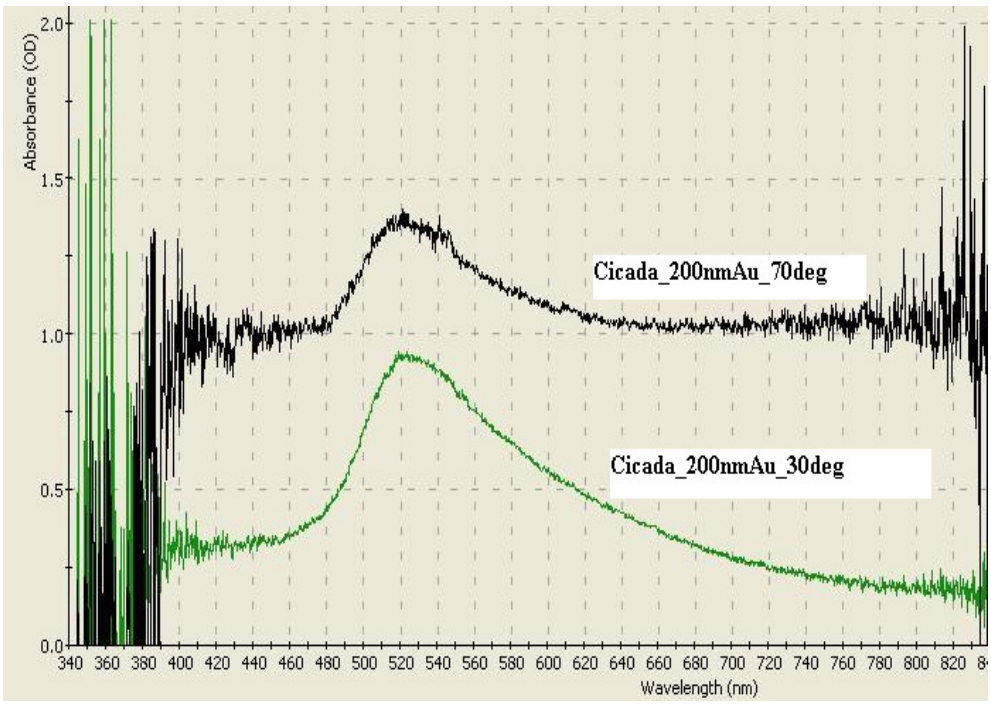

Figure 5.9: Spectra for two different angle of Au film deposition on cicada

5.8 Plasmon resonance of silver (Ag) nanoparticles

Having successfully obtained plasmon resonance effect and also size variation for Au nanoparticle array, it was decided to test an Ag array as well. Electron beam deposition technique was used for the deposition of Ag nanoparticle..

5.8.1 Methodology of deposition

Sections of wing from cicada were coated with a 65nm layer of silver (99.99%) in an electron beam deposition system. The deposition was controlled by a quartz crystal microbalance. The sample was coated such that the surface normal was parallel to the vapour flux. The coating was intended to generate reasonably isolated metal particles, in analogy with the approach of White (2006) et al.

Since this particular experiment obtains result further into UV range, deuterium lamp source as discussed in section 3.2 was used in conjunction with the halogen lamp. Absorbance spectroscopy was carried out and spectrum obtained.

5.8.2 Results

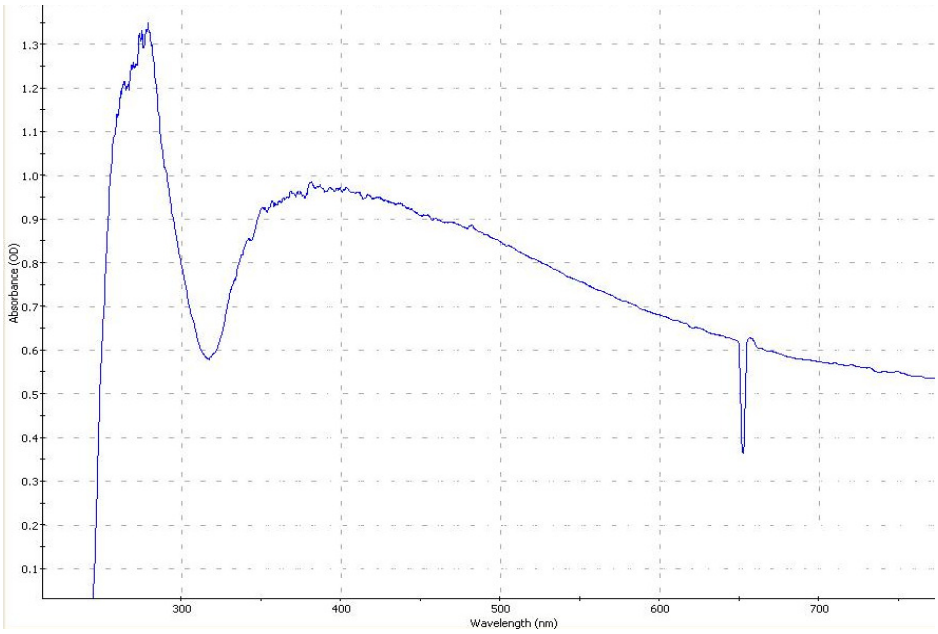

Figure 5.10: Plasmon resonance peak obtained at 65nm for Ag NP

The surface plasmon resonance peak for 65nm Ag nanoparticle array is shown in figure 5.10 and it is observed to lie in the vicinity of 400nm, approximately 380nm.

5.8.3 Discussion

The plasmon resonance frequency peak for Ag array was verified by (Mishra, 2007). It is to be noted that the peak obtained below 300nm looks to appear more due to noise in the system than actual plasmon resonance. A sharp dip around 650nm is understood to be due to a defect state in the array.

5.8.4 Applications of surface plasmon resonance

Surface plasmons have been used to enhance the surface sensitivity of several spectroscopic measurements including fluorescence, Raman scattering (SERS), and second harmonic generation. However, in their simplest form, SPR measurements can be used to detect DNA or proteins by the changes in the local index of refraction upon adsorption of the target molecule to the metal surface. Thus, an important application of SPR is in the development of bio-sensors. An important consequence of using gold for surface Plasmon based sensors is that due to permittivity of gold, sensing is usually limited to visible and near-infrared part of spectrum. Besides, gold establishes bonds with organic molecules with relative ease (Maier, 2007).

For nanoparticles, localized surface plasmon oscillations can give rise to the intense colors of solutions of plasmon resonance nanoparticles and/or very intense scattering.

5.9 SERS measurements

5.9.1 Introduction

This technique is a variant of raman spectroscopy and is useful for obtaining raman spectrums of weak adsorbates. Enhacement in intensity can be as high as 10^{14}. To obtain SERS of the adsorbate, it is adsorbed on the adsorbent, which is the metal nanostructure array discussed so far for plasmon resonance effect. In this experiment, thiophenol was taken as the adsorbate as it provides a convenient reference compound

for SERS. It is known to form relatively stable monolayers on silver and gold metal surfaces (Kneipp, 1999).

5.9.2 Methodology

In order to evaluate the SERS capability of the silver nanoparticle array, the sample was soaked in a 10mM solution of thiophenol (99+%, Sigma-Aldrich) in ethanol (>99.7%, Merck) for 10min. Soaking was followed by a rinse in pure ethanol for 2min.

5.9.3 Results

The SERS spectrum is shown in figure 5.11.

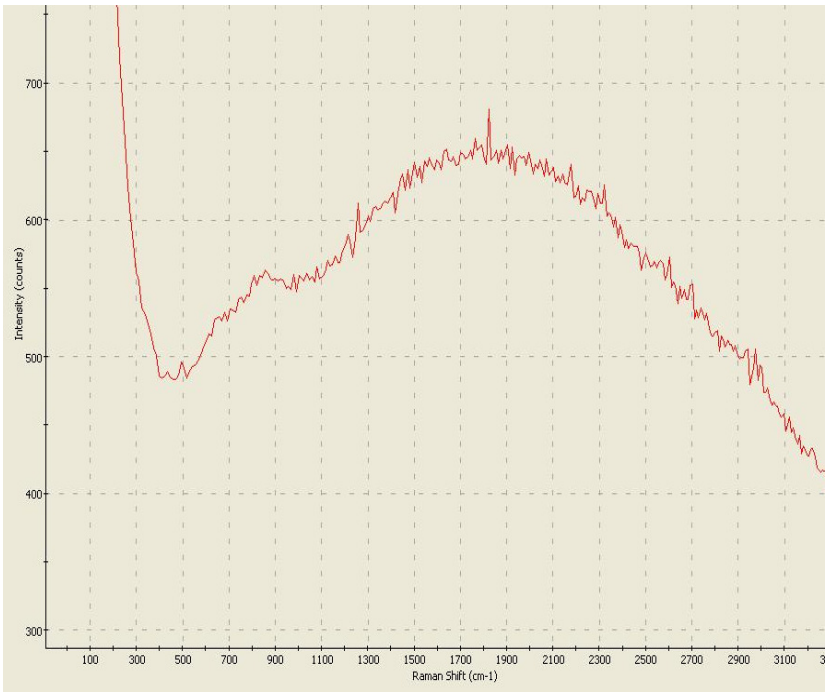

Figure 5.11: SERS result obtained from the Ag array with thiophenol adsorbed

5.9.4 Discussion

Unfortunately, the spectrum was shown to comprise of large fluorescence background and didn't show well resolved raman peaks. Research is underway to investigate whether this shortcoming happened due to preparation of the sample for SERS or due to instrumentation failures.

5.10 Conclusion

The 'Plasmon resonance effect' for a metal nanoparticle array (both gold and silver) on a biological nanostructured substrate was obtained experimentally. Also, the effect of size of nanoparticles on the position of absorbance peak was obtained and discussed with the help of due reference from the literature.

An attempt has also been made to obtain 'Surface Enhanced Raman Scattering' by adsorbing thiophenol, a weak adsorbate for raman but a convenient compound for SERS. Although the result obtained was poor in many aspects but it provided a future research direction nevertheless.

Chapter 6 Conclusions

6.1 Summary of Research Contribution

The research discussed in this thesis has accomplished the objectives put forth in chapter 1. Experiments carried out have led to the following objectives being met:

1. In chapter 3, polyaniline nanofibers were fabricated by means of two techniques, chemical and electro-chemical polymerization. The nanofibers obtained by chemical polymerization technique were unordered and uneven whereas, electropolymerization was verified by SEM and TEM images to produce well distinguishable strands of fibers having diameters in the range 30-50nm and lengths stretching through a few micrometers.

2. UV-Visible spectroscopy technique was developed and used to investigate the effect of doping the nanofiber films on the optical properties, under different conditions of oxidation potentials, electrolytic environment and temperature. Using transmission and absorbance spectroscopy, PANI nanofibers was found to change oxidation states and color in a reversible manner.

3. In chapter 4, UV-Visible spectroscopy was taken one step ahead and improved into a more sophisticated form called raman spectroscopy. The instrumentation provided acceptable results for the samples of paracetamol and polystyrene. The results were found to match well with the published reports as far as the observation of raman peaks is concerned. Optical resolution and sensitivity were distinguished to be areas of improvement but cost effectiveness and portability of the developed instrumentation was a major accomplishment. The cost of the system was only few thousand dollars compared to modern day systems which can cost hundreds of thousands.

4. Chapter 5 utilized both optical spectroscopy techniques to investigate nano-scale structures of a different kind. Gold and silver films were successfully fabricated in

the form of 3-D nano-particle arrays, on a biological nano-structures substrate. The deposition was verified by the SEM images obtained. Both nano-arrays were observed using absorbance spectroscopy to produce 'surface plasmon resonance' frequency bands. The position of the band was observed to be a function of the size of Au nanoparticles.

5. SERS capability of the metal array was tested for a weak raman adsorbate (thiophenol), but the result obtained was disappointing. It was found to consist of large fluorescence band. It thus provides an area of future work.

6.2 Probable Future Works

Major areas of work that are earmarked for possible future endeavours are discussed here:

1. Work on polyaniline could be extended to its applications say for the development of electrochromic windows. These windows would be used like normal windows in buildings and will determine the amount of sunlight to let through at different times during the day. These would help bring down the energy requirements by controlling the illumination and temperature levels in the room these are installed in.

2. More work could be done on raman instrumentation to improve its features and incorporate other variations of raman spectroscopy such as Resonance Raman, SERS, Spontaneous Raman Spectroscopy, Stimulated Raman Spectroscopy and Coherent anti-Stokes Raman spectroscopy (CARS).

3. SERS is an important form of Raman spectroscopy. The exact mechanism of the enhancement effect of SERS is still a matter of debate in the literature, so it gives a lot of scope for future research endeavors. It's been investigated in this research but the results obtained are not so satisfactory. This could be due to poor detector sensitivity or may be due to poor sample preparation. This work could be extended to obtaining different shapes and sizes of nanoparticles.

REFERENCES

"Introduction to Raman spectroscopy", Perkin Elmer, 2007.

Aliganga A.K.A., Lieberwirth I., Glasser G., Duwez A., Sun Y., Mittler S., Organic Electronics, 2006

Al-Zoubi N, Koundourellis J.E., Malamataris S., Journal of Pharmaceutical and Biomedical Analysis, Vol. 29, pp. 459–467, 2002.

Aoki K., Teragishi Y.J., Electroanalytical Chemistry, Vol. 441, pp.25, 1998.

Aussawasathien D., Dong J.H. and Dai L., *Synthetic Metals*, Vol. 154, no. 1–3, pp. 37–40, 2005.

Barta P., Kugler T., Salaneck W.R., Monkman, A.P., Libert J., Lazzaroni R., Bredas J.L., Synth Met, Vol. 93, pp.83, 1998.

Bell S.E.J., Bourguignon E.S.O. and Dennis A., Analyst, Vol.123, pp.1729–1734, 1998.

Bell S.E.J., Bourguignon E.S.O., Dennis A., Fields J.A., McGarvey J.J. and Seddon K.R., Analytical Chemistry, Vol. 72, pp. 234-239, 2000.

Berciaud S., Cognet L., Tamarat P. and Lounis B., Nano Lett., Vol.5, pp.515- 8, 2005.

Chen S.A., Chuang K.R., Chao C.I. and Lee H.T., Synthetic Metals, Vol.82, pp.207-210, 1996.

Choi B., Lee H., Jin S., Chun S. and Kim S., Nanotechnology, Vol. 18, pp. 075706-075711, 2007

Daniel M. and Astruc D., Chem. Rev., Vol.104, pp.293-346, 2004

Day J.S., Edwards H.G.M., Dobrowski S.A. and Voice A.M., Spectrochimica Acta Part A, Vol.60, pp.563–568, 2004.

Debarnot, D.N.; Epaillard, F.P. Polyaniline as a new sensitive layer for gas sensors. Analytica Chimica Acta, Vol.*475*, pp.1–15, 2003.

Djurado, D, Bee, M., Gonzalez M., Mondelli C., Dufour B., Rannou P., Pron A. and Travers J. P., Chemical Physics, Vol. 292, pp.355, 2003.

Dollish F.R., Fateley W.G. and Bentley F.F., "Characteristic Raman frequencies of Raman Compounds", Wiley Inter-Science, New York, 1974.

Fahrner W.R.,"Nanotechnology and Nanoelectronics: Materials, Devices, Measurement Techniques", Springer, 2004.

Fleischmann M., Hendra P.J. and MacQuillan A.J., Chemical Physics Letters, Vol.26, pp.63, 1974.

Freeman S.K., "Applications of Laser Raman Spectroscopy", Wiley Inter-Science, New York, 1974.

Goser. K., "Nanoelectronics and Nanosystems: From Transistors to Molecular and Quantum Devices", Springer, 2004.

Grasselli J.G., Snavely M.K. and Bulkin B.J., Physics Reports (review section of Physics Letters), Vol. 65, No. 4, pp. 231-344, 1980.

Huang J. and Kaner R.B., Journal of American Chemical Society, Vol. 126, pp. 851-855, 2004.

Hutter E., Fendler J., Exploitation of Localised Syrface Plasmon Resonance, Advanced Materials, Vol 16(19), pp.1685, 2004.

Kachrimanis K., Braun D.E. and Griesser U.J., Journal of Pharmaceutical and Biomedical Analysis, Vol. 43, pp. 407–412, 2007.

Kelly K.L., Coronado E., Zhao L.L. and Schatz G.C., Jounral of Physical Chemistry B, Vol. 107, pp. 668-77, 2003.

Klar T., Perner M., Grosse S., Plessen G.V., Spirkl W. and Feldmann J., Physical Review Letters, Vol. 80, No. 19, p.4249, 1998.

Kneipp K., Kneipp H., Itzkan I., Dasari R. and Feld M., Chemical Review, Vol. 99, pp. 2957, 1999.

Kossyrev P.A., Yin A., Cloutier S.G., Cardimona D.A., Huang D., Alsing P.M. and Xu J. M., Nano Lett., Vol.5, pp.1978-81, 2005.

Kreibig U., Genzel L., Surface Science, Vol. 156, pp. 678-700, 1985.

Lam T., "A New Era in Affordable Raman Spectroscopy" Raman Technology for Today's Spectroscopists, June 2004.

Li Y.X., Hagen J and Haarer D., Synthetic Metals, Vol. 94, pp. 273, 1998.

Liang E.J., Ye X.L. and Kiefer W., Journal of physical Chemistry A , Vol. 101, pp. 7330-7335, 1997

Libert J., Cornil J., dos-Santos D.A., Bredas J.L., Physical Review B, Vol. 56, pp. 8638, 1997.

Lin-Vien, D., Colthup N.B., Fateley W.B. and Graselli J.G., "The Handbook of Infrared and Raman Characteristic Frequencies of Organic Molecules", Academic Press: Boston, 1991.

Liu J., Cankurtaran B., WieczorekL., Ford M.J. and Cortie M., Advanced Functional Materials, Vol. 16, pp. 1457–1461, 2006.

Liu J., Lin Y., Liang L., Voigt J.A., Hunber D.L., Tian Z.R.,Coker E., McKenzie B. and McDermott M. J., Chemical European Journal, Vol. 9, pp. 604, 2003.

Long D.A., "Raman Spectroscopy", Mc-Graw Hill, 1977.

MacDonald A.M. and Wyeth P., Journal of Raman Spectroscopy, Vol. 37, 2006

McCall R.P., Leng L.M., Ye H.J., Manohar S.K., Masters J.G., Asturias G.E., MacDiarmid A.G. and Epstein A.J., Physical Review B, Vol. 41, pp. 5202, 1990.

McCreery R.L., "Photometric Standards for Raman Spectroscopy", John Wileys & Sons Ltd, 2002.

Mishra Y.K., Mohapatra S., Kabiraj D., Mohanta B., Lalla N.P., Pivin J.C. and Avasthi D.K., Scripta Materialia, Vol. 56, pp. 629–632, 2007.

Moskovits M., Rev. Mod. Phys., Vol. 57(3): Part 1, pp. 783, 1985

Moynihan H.A. and O'Hare I.P., International Journal of Pharmaceutics, Vol. 247, pp.179-185, 2002.

Mulvaney P., Langmuir, Vol. 12, pp. 788-800.

Pałys B., Celuch P., Electrochimica Acta, Vol. 51, pp. 4115–4124, 2006.

Pitt G.D., Batchelder D.N., Bennett R., Bormett R.W., Hayward I.P., Smith B.J.E., Williams K.P.J., Yang Y.Y., Baldwin K.J. and Webster S., IEE Proceedings-Science, Measurement and Technology , Vol. 152, Issue 6, pp. 241–318, 2005.

Raman C.V., and Krishnan K.S., "A new type of secondary radiation", Nature, 1928, Vol.121, p. 501

Robinson J.W., Frame E.M.S. and Frame G.M., "Undergraduate instrumental analysis", 2004.

Rechberger W., Hohenau A., Leitner A., Krenn J.R., Lamprecht B., Aussenegg F.R., Optical properties of two interacting gold nanoparticles, Optics Communications, Vol. 220, pp. 137–141, 2003

Sabatani E., Gafni Y. and Rubinstein I., Journal of Physical Chemistry, Vol.99, pp.12305, 1995.

Sadek A.Z., Baker C.O., Powell D.A., Wlodarski W., Kaner R.B. and Kalantar-zadeh K., IEEE Sensors Journal, Vol.7, Issue 2, pp. 213-218, 2007.

Sarno D.M., Manohar S.K. and MacDiarmid A.G., Synthetic Metals, Vol. 148, pp. 237–243, 2005.

Schreiber M., Tenelsen K. and Vojt T.J., Luminescence, Vo. 66/67, pp.521, 1996.

Sengupta P.P., Barik S. and Adhikari B., Materials and Manufacturing Processes, Vol. 21, pp. 263–270, 2006.

Sherry L.J., Chang S., Schatz G.C., Van Duyne R.P., Wiley B.J. and Xia Y., Localized Surface Plasmon Resonance Spectroscopy of Single Silver Nanocubes, Nano letters, Vol. 5(10), pp. 2034-8, 2005.

Smith E. and Dent G., "Modern Raman Spectroscopy: A Practical Approach", February 2005.

Thach G.N., Mitchell A., Journal of Lightwave Technology, Vol. 24, Issue 1, p. 635, 2006

Thorley F.C., Baldwin K.J., Lee D.C. and Batchelder D.N., Journal of Raman Spectroscopy, Vol. 37, pp. 335–341, 2006.

Vaughan A.S., Dodd S.J. and Sutton S.J., Vol.39, pp. 181– 191, 2004.

Virji S., Fowler J.D., Baker C.O., Huang J., Kaner R.B. and Weiller B.H., *Small*, Vol. 1, no. 6, pp. 624–627, 2005.

Waser R., "Nanoelectronics and Information Technology", John Wiley & Sons, New York, 2005.

Watson G.S. and Blach J.A., in Proceedings of SPIE: Smart Materials II, Vol. 4934, SPIE Press, Bellingham, p. 378, 2002 .

Wennerstrom O., Macromolecules, Vol.18, pp.1977, 1985.

Xu H., Aizpurua J., Ka¨ll M. and Apell P., Electromagnetic contributions to single-molecule sensitivity in surface-enhanced Raman scattering, Vol. 62(3), pp. 4318, 2000.

Yu X.F., Li Y.X., Zhu N.F., Yang Q.B. and Kalantar-zadeh K., Nanotechnology, Vol. 18, pp. 015201-015208, 2007.

Zhang G., Zhang J., Xie G., Liu Z. and Shao H., Small , Vol. 2, No.12, pp.1440 – 1443, 2006.

Zhekova H., Tadjer A., Ivanova A., Petrova J. and Gospodinova N., International Journal of Quantum Chemistry, Vol. 107, pp. 1688–1706, 2007.

APPENDIX

A) Characteristic frequencies for bond recognition using Raman and Infra-red Spectroscopy [Kreibig(1985)].

Characteristic wavenumbers and Raman and infrared intensities of groups in organic compounds. (From ref. [2].)

Vibration[a]	Region (cm^{-1})	Intensity[b]	
		Raman	Infrared
ν(O–H)	3650–3000	w	s
ν(N–H)	3500–3300	m	m
ν(≡C–H)	3300	w	s
ν(=C–H)	3100–3000	s	m
ν(–C–H)	3000–2800	s	s
ν(–S–H)	2600–2550	s	w
ν(C≡N)	2255–2220	m–s	s–0
ν(C≡C)	2250–2100	vs	w–0
ν(C=O)	1820–1680	s–w	vs
ν(C=C)	1900–1500	vs–m	0–w
ν(C=N)	1680–1610	s	m
ν(N=N), aliphatic substituent	1580–1550	m	0
ν(N=N), aromatic substituent	1440–1410	m	0
ν_a((C–)NO_2)	1590–1530	m	s
ν_s((C–)NO_2)	1380–1340	vs	m
ν_a((C–)SO_2(–C))	1350–1310	w–0	s
ν_s((C–)SO_2(–C))	1160–1120	s	s
ν((C–)SO(–C))	1070–1020	m	s
ν(C=S)	1250–1000	s	w
$\delta(CH_2)$, $\delta_a(CH_3)$	1470–1400	m	m
$\delta_s(CH_3)$	1380	m–w, s, if at C=C	s–m
ν(CC), aromatics	1600, 1580	s–m	m–s
	1500, 1450	m–w	m–s
	1000	s (in mono-; *m*-; 1,3,5-derivatives)	0–w
ν(CC), alicyclics, and aliphatic chains	1300–600	s–m	m–w
ν_a(C–O—C)	1150–1060	w	s
ν_s(C–O–C)	970–800	s–m	w–0
ν_a(Si–O–Si)	1110–1000	w–0	vs
ν_s(Si–O–Si)	550–450	vs	w–0
ν(O–O)	900–845	s	0–w
ν(S–S)	550–430	s	0–w
ν(Se–Se)	330–290	s	0–w
ν(C(aromatic)–S)	1100–1080	s	s–m
ν(C(aliphatic)–S)	790–630	s	s–m
ν(C–Cl)	800–550	s	s
ν(C–Br)	700–500	s	s
ν(C–I)	660–480	s	s
δ_s(CC), aliphatic chains			
C_n, $n = 3, \ldots, 12$	400–250	s–m	w–0
$n > 12$	$2495/n$		
Lattice vibrations in molecular crystals (librations and translational vibrations)	200–20	vs–0	s–0

[a] ν stretching vibration, δ bending vibration, ν_s symmetric vibration, ν_a antisymmetric vibration.

[b] vs very strong, s strong, m medium, w weak, 0 very weak or inactive.

B) Theoretical calculations defining plasmon resonance effect with decreasing size of nanoparticle [Kreibig(1985)].

Table 1
Plasma peak positions: theories

	Ref.	Shift with decreasing R
(1) Maxwell theory;		
Drude dielectric function		
with free path limitation	[4]	Red
with diffuse surface layer	[12]	Red
with substrate interaction	[13]	Red
with additional boundary condition (ABC)	[14,15]	Blue
with dielectric cores	[16]	Red or blue (depending on ϵ_{core})
(2) Discrete energy levels;		
linear response	[17,18]	Blue
with surface states and interband transitions	[19]	Blue (red)
(3) Quantum box model;		
RPA	[5]	Blue
	[20]	Red
improved	[21]	Blue + oscillation
(4) Thomas–Fermi approximation;		
sum rule	[22]	Blue
(5) Jellium; local density;		
self-consistent	[23]	Red
(6) Hydrodynamical model;	[24]	Blue
diffuse electron density	[25]	Red (smooth)
profile		Blue (step)
	[26]	Red
	[27]	Red
(7) Nonlocal effects	[28]	

C) Material size effects defining plasmon resonance shifts with decreasing size of nanoparticles [Kreibig(1985)].

Table 2
Additional material size effects

	Ref.	Broadening and shift with decreasing R
(1) Lattice contractions; Influences on the conduction electron density	[29–32]	Blue-shift (Ag particles: volume contraction $\Delta V/V \approx 5\%$ shift ≈ 0.1 eV)
(2) Changes of the effective mass of the conduction electrons		Increase: red-shift Decrease: blue-shift
(3) Changes of electronic band structure	Ag: [33,34] Au: [35]	
(4) Changes of optical interband transitions	Au: [36] Ag: [37]	Blue-shift Blue-shift
(5) Additional "molecular" absorption structures in samples with a distribution of particle sizes	Ag: [5,38–41]	Blue-shift broadening
(6) Deviations of the embedding medium $-\epsilon$ from the mean value near the particle interface (adsorption layers, ion enrichment, etc.)	[42]	Increase: red-shift Decrease: blue-shift
(7) Rough particle–matrix interface	See fig. 4	Au: red-shift broadening
(8) Physisorption/chemisorption/ chemical reactions at the interface		?
(9) Asymmetric plasma band shapes (R dependent)	See fig. 5	Ag: blue-shift

PUBLICATIONS

- Qasim H., Sadek A.Z., Arsat R., Wlodarski W., Belski I., Kaner R.B. and Kalantar-zadeh K., "Optical and Conductivity dependence on doping concentration of polyaniline nanofibers", in Proceedings of SPIE Conference (Microelectronics, MEMS and Nanotechnology), Canberra, Australia, 4-7 December 2007.
- Work was also presented as part of 'Research Methods' course which was a module of the research and also at a school conference at RMIT University in Sept' 07.